Characteristics of intercontinental transport of tropospheric ozone from Africa to Asia

Han Han[1], Jane Liu[1,2], Huiling Yuan[1], Bingliang Zhuang[1], Ye Zhu[1,3], Yue Wu[1], Yuhan Yan[4], Aijun Ding[1]

[1]School of Atmospheric Sciences, Nanjing University, Nanjing, China

[2]Department of Geography and Planning, University of Toronto, Toronto, Canada

[3]Shanghai Public Meteorological Service Centre, Shanghai, China

[4]Chinese Academy of Science, Institute of Atmospheric Physics, Beijing, China

Correspondence to: Jane Liu (janejj.liu@utoronto.ca)

Abstract.

In this study, we characterize the transport of ozone from Africa to Asia through the analysis of the simulations of a global chemical transport model, GEOS-Chem, from 1987 to 2006. The receptor region Asia is defined within 5°N-60°N and 60°E-145°E, while the source region Africa is within 35°S-15°N and 20°W-55°E and within 15°N-35°N, 20°W-30°E. The ozone generated in the African troposphere from both natural and anthropogenic sources is tracked through tagged ozone simulation. Combining with analysis of trajectory simulations using the Hybrid Single-Particle Lagrangian Integrated Trajectory model, we find that the upper branch of the Hadley cell connects with the subtropical westerlies in the northern hemisphere (NH) to form a primary transport pathway from Africa to Asia in the middle and upper troposphere throughout the year. The Somali Jet that runs from eastern Africa near the equator to the Indian subcontinent in the lower troposphere is the second pathway that appears only in NH summer.

The influence of African ozone mainly appears over Asia south of 40°N. The influence shows strong seasonality, varying with latitude, longitude, and altitude. In the Asian upper troposphere, imported African ozone is largest from March to May around 30°N (12-16 ppbv) and lowest during July-October

around 10°N (~2 ppbv). In the Asian middle and lower troposphere, imported African ozone peaks in NH winter between 20-25°N. Over 5-40°N, the mean fractional contribution of imported African ozone to the overall ozone concentrations in Asia is largest during NH winter in the middle troposphere (~18%) and lowest in NH summer throughout the tropospheric column (~6%).

This seasonality mainly results from the collective effects of the ozone precursor emissions in Africa, and meteorology and chemistry in Africa and Asia and along the transport pathways. The seasonal swing of the Hadley circulation and subtropical westerlies along the primary transport pathway play a dominant role in modulating the seasonality. There is more imported African ozone in the Asian upper troposphere in NH spring than in winter. This is likely due to more ozone in the NH African upper troposphere from biogenic and lightning NO_x emissions in NH spring. The influence of African ozone on Asia appears larger in NH spring than in autumn. This can be attributed to stronger subtropical westerlies and higher altitudes of the elevated ozone in Africa in NH spring. In NH summer, African ozone hardly reaches Asia because of the blockings of Saharan High, Arabian High, and Tibetan High on the transport pathway in the middle and upper troposphere, in addition to the northward swing of the subtropical westerlies. The seasonal swings of the Intertropical Convergence Zone (ITCZ) in Africa, combining with the geographic variations in emissions with season, can further modulate the seasonality of the transport of African ozone owing to the functions of the ITCZ in enhancing lightning NO_x generation and uplifting ozone and ozone precursors to upper layers. The strength of the ITCZ in Africa is also found to be positively correlated with the interannual variation of the transport of African ozone to Asia in NH winter.

Ozone from NH Africa makes up over 80% of the total imported African ozone over Asia in most altitudes and seasons. The interhemispheric transport of ozone from the southern hemispheric Africa is most evident in NH winter over the Asian upper troposphere and in NH summer over the Asian lower troposphere. The former case is associated with the primary transport pathway in HW winter, while the

latter case is with the second transport pathway. The intensities of the ITCZ in Africa and the Somali jet can respectively explain ~30% of the interannual variations in the transport of ozone from the southern hemispheric Africa to Asia in the two cases.

1 Introduction

Tropospheric ozone is a major air pollutant, harmful to human health (Anenberg et al., 2010), agricultural crops, and natural ecosystems (Hollaway et al., 2012; Lefohn et al., 2017). It also acts as a greenhouse gas, whose global mean radiative forcing is about 0.4 ± 0.2 W/m^2 for the period 1750-2011 (Myhre et al., 2013). The dominant source of tropospheric ozone is from the photochemical reactions in which volatile organic compounds (VOCs) and carbon monoxide (CO) are oxidized in the presence of nitrogen oxides (NO$_x$) (Lelieveld and Dentener, 2000). Transport of ozone from the stratosphere downward is another source of tropospheric ozone (Neu et al., 2014; Akritidis et al., 2016). Due to its lifetime of days to weeks in the free troposphere, ozone can be transported over long distances across continents, as shown in a wealth of observation evidence (Huntrieser et al., 2005; Lewis et al., 2007; Verstraeten et al., 2015). Consequently, tropospheric ozone in a region is greatly influenced by ozone transport from upwind regions (Doherty et al., 2013, 2017). Therefore, intercontinental transport of ozone has been a significant issue to scientists, public, and policymakers concerned with air quality and climate change (HTAP, 2010; Cooper et al., 2015; Doherty, 2015; Huang et al., 2017).

There have been numerous studies on the major source-receptor relationships in the northern hemisphere (NH) for ozone transport among Asia, North America, and Europe, which are trans-Pacific (Jaffe et al., 2003; Zhao et al., 2003; Cooper et al., 2010; Nopmongcol et al., 2017), trans-Atlantic (Wild et al., 1996; Cooper et al., 2002; Guerova et al., 2006; Derwent et al., 2015; Karamchandani et al., 2017; Knowland et al., 2017), and trans-Eurasian (Wild et al., 2004; Fiore et al., 2009; Li et al., 2014b) transport. The trans-Pacific transport from Asia to North America has been studied most because of the

efficient eastward export of high pollutants in Asia and the close connection to legislative issues related to the control of ozone in USA (Cooper et al., 2010, 2011, 2015; Verstraeten et al., 2015; Huang et al.,

75   2017; Lin et al., 2017). Developing a better understanding of the intercontinental transport of ozone across the NH is one of the main objectives for the Task Force on Hemispheric Transport of Air Pollution (TF HTAP) (Galmarini et al., 2017, http://www.htap.org).

Transport of ozone to Asia from various source regions in the world has been less documented but received increasing attention since the 2000s (Holloway et al., 2008; Nagashima et al., 2010; Wang et

80   al., 2011; Li et al., 2014b; Chakraborty et al., 2015; Zhu et al., 2016; Zhu et al., 2017b). The distribution of foreign ozone in Asia is modulated by numerous processes, involving chemistry and meteorology in both Asia and the various source regions, as well as along the transport pathways (Wild et al., 2004; Li et al., 2014b). Previous studies illustrated the important role that meteorology plays in these processes (Sudo and Akimoto, 2007; Sekiya and Sudo, 2012, 2014; Zhu et al., 2017b). For example, governed by

85   the westerlies in the NH, the influence of European and North American ozone on Asia is larger in higher latitudes than in lower altitudes (Wild et al., 2004; Holloway et al., 2008; Zhu et al., 2017b). The seasonal switch in Asian monsoonal winds significantly affects the seasonal variation of ozone transported to Asia (Nagashima et al., 2010; Wang et al., 2011; Zhu et al., 2017b). The Asian monsoon anticyclone (South Asian High, SAH) can also modulate the movement of ozone in the upper

90   troposphere over Eurasia (Vogel et al., 2014; Garny and Randel, 2016).

Africa covers areas from the NH to the Southern Hemisphere (SH), with around three quarters of the continent in the tropics. Comparing with other continents, Africa has the most frequent lightning (Albrecht et al., 2016) and the largest burned areas (Giglio et al., 2013). Approximately, 70% of tropospheric ozone produced over the African troposphere is exported out of Africa (Aghedo et al.,

95   2007), making African ozone an obvious influence on the global tropospheric ozone budget (Piketh and Walton, 2004; Thompson, 2004; Williams et al., 2009; Bouarar et al., 2011; Zare et al., 2014).

Nevertheless, there is relatively little literature on the transport of African ozone to Asia (Liu et al., 2002; Sudo and Akimoto, 2007; Lal et al., 2014). By tagging ozone from Africa in a global chemistry transport model, Liu et al. (2002) reported that African ozone contributed about 10-20 ppbv to the overall ozone concentrations in the middle and upper troposphere at Hong Kong, China, during the November-April period. Sudo and Akimoto (2007) showed that there is a significant interhemispheric ozone transport from South America to Japan in the upper troposphere in conjunction with ozone export from northern Africa. Lal et al. (2014) reported that the ozone distribution over western India in the lower troposphere during the summer monsoon season is affected by long-range transport from the east coast of Africa. These previous studies mostly focused on the transport of African ozone to some locations in Asia. It is unclear to which degree that African ozone influences Asia regionally, how the transport pathways vary with season, and what underlying mechanisms modulate the transport.

The Intertropical Convergence Zone (ITCZ), defined as the convergence of the trade winds, is one of the most prominent meteorological phenomena in the tropics (Waliser and Gautier, 1993; Žagar et al., 2011; Suzuki, 2011). ITCZ is a heat engine driving the ascending branch of the Hadley circulation (Nicholson, 2009; Suzuki, 2011). ITCZ and its seasonality can significantly impact the meteorological conditions over Africa (Nicholson, 2009; Collier and Hughes, 2011; Suzuki, 2011). Characterized with deep and strong convection, the equatorial region between the ITCZ branches is a region with effective interhemispheric mixing (Avery et al., 2001). The convective divergence in the upper troposphere over the ITCZ was proposed to be one of the primary mechanisms for the interhemispheric transport (Hartley and Black, 1995; Avery et al., 2001). Meanwhile, the ITCZ can be a barrier to interhemispheric exchange in the lower troposphere (Raper et al., 2001). Together with the Southeast Asian monsoon, the movement of the ITCZ can modulate pollution transport to Southeast Asia (Pochanart et al., 2003, 2004). In addition, the ITCZ over western Africa is found to play a significant role in controlling the transport of Saharan mineral dust to northern South America, modifying air quality and climate there

(Piketh and Walton, 2004; Doherty et al., 2012, 2014; Rodríguez et al., 2015). However, the influence of the ITCZ on ozone transport from Africa to Asia has not been well understood.

In this paper, we present a comprehensive study on the transport of African ozone to Asia through analysis of tagged ozone simulations, as well as trajectory simulations. In this paper, the term "African ozone" refers to ozone that is generated in the African troposphere below the tropopause from both natural and anthropogenic sources, as Sudo and Akimoto (2007) suggested that investigating the contributions of both sources to ozone production is necessary. The term "imported African ozone" or "imported ozone" refers to the African ozone that has reached and distributed over Asia, and it refers to African ozone concentrations in model grids in Asia. The source region Africa and the receptor region Asia are shown in Fig. 1. The contribution of the source regions to the receptor region is presented as absolute or fractional contribution. The former refers to the imported African ozone concentrations in ppbv, while the latter is the ratio of the imported ozone concentrations to the overall ozone concentrations in a grid, a layer, or a region in Asia. Our specific objectives are (1) to characterize the seasonal variation of ozone transport from Africa to Asia, (2) to investigate the underlying mechanisms responsible for such seasonal variation, and (3) to find the meteorological influences, including the ITCZ, on the interannual variations of the transport of African ozone to Asia, including interhemispheric transport from the SH. Our analysis is based on the simulations from a 3-dimensional global chemical transport model, GEOS-Chem (Bey et al., 2001a), for 20 years from 1987 to 2006, supplemented by the analysis of trajectory simulations from the Hybrid Single-Particle Lagrangian Integrated Trajectory model (HYSPLIT) (Draxler and Hess, 1998; Stein et al., 2015). In section 2, GEOS-Chem and the tagged ozone stimulation method are described, followed by the comparison of GEOS-Chem simulations with ozonesonde and satellite data. The HYSPLIT model and the meteorological data are also described. Section 3 is the core section that discusses the seasonality of imported African ozone over Asia and possible underlying mechanisms. In section 4, the meteorological influence on in

145   interannual variation in the transport of African ozone to Asia, including the interhemispheric transport,

is explored from the perspective of meteorological influences. Finally, conclusions are drawn in section

5.

2 Models and data

2.1 The description of the GEOS-Chem model

150 A global 3-dimensional chemistry transport model, GEOS-Chem (version v9-02) (Bey et al., 2001a,

http://geos-chem.org), is employed to simulate the global ozone distributions and the source-receptor

relationship between Africa and Asia. GEOS-Chem includes a detailed description of tropospheric O_3-

NO_x-hydrocarbon-aerosol. It is driven by assimilated meteorological data from the GEOS at NASA

155 Global Modeling and Assimilation Office (GMAO).

In this study, the simulations are driven by GEOS-4 meteorology at a 4° latitude by 5° longitude

horizontal resolution, degraded from their native resolution of $1°$ latitude by $1.25°$ longitude. There are

30 vertical layers including 17 levels in the troposphere. Transport and chemical timesteps are 10

minutes and 20 minutes, respectively, as suggested by Philip et al. (2016). GEOS-4 uses the deep

160 convection scheme of Zhang and McFarlane (1995) and the shallow convection scheme of Hack (1994).

By comparing the GEOS-Chem simulations driven by GEOS-4 and GEOS-5 with satellite observations

in the tropical troposphere, Liu et al. (2010) and Zhang et al. (2011) have found GEOS-4 has stronger

deep convection in the tropics than GEOS-5. In general, GEOS-Chem driven by GEOS-4 can simulate

tropospheric ozone that is in good agreement with ozonesonde observations (Liu et al., 2010; Zhang et

165 al., 2011; Choi et al., 2017; Zhu et al., 2017b).

GEOS-Chem has various modes that serve different simulation goals. In the full chemistry

simulation, the emission inputs for a specific year are scaled from each inventory's base year. The

global anthropogenic emission inventories are from EDGAR 3.2 for NO_x, CO, SO_x in a base year 2000

(Olivier and Berdowski, 2001) and RETRO for VOC emissions (Pulles et al., 2007) in 2000, merged with the following regional inventories: the INTEX-B Asia emissions inventory in 2006 (Zhang et al., 2009), the US Environmental Protection Agency National Emission Inventory in 2005 (NEI05) for North America, the Cooperative Programme for Monitoring and Evaluation of the Long-range Transmission of Air Pollutants in Europe (EMEP) inventory for Europe (Vestreng and Klein, 2002) in 2005, Big Bend Regional Aerosol and Visibility Observational (BRAVO) Study Emissions Inventory for 1999 in Mexico (Kuhns et al., 2003), and the Criteria Air Contaminants (CAC) inventory for Canada in 2005. Biofuel emission inventory is from Yevich and Logan (2003). Biomass burning and Biogenic emissions are from the GFED3 inventory (van der Werf et al., 2010) and MEGAN 2.1 (Guenther et al., 2012) respectively. Lightning NO_x emissions are calculated with the scheme of Allen et al. (2010) and the vertical distribution suggested by Ott et al. (2010). The annual global lightning NO_x emissions is 5.97 Tg N yr^{-1}, comparable to 6±2 Tg N yr^{-1} in Martin et al. (2007) and 6.3 Tg N yr^{-1} in Miyazaki et al. (2014). The annual total lightning NO_x emission in Africa is 1.6 Tg N yr^{-1}, 0.80 Tg N yr^{-1} in NHAF, and 0.79 Tg N yr^{-1} in SHAF, shown in Figs. S1 and S2. The anthropogenic CO and NO_x emissions from GEOS-Chem for 2000 are compared with those in the HTAP2 emission inventories for 2008 (http://edgar.jrc.ec.europa.eu/htap_v2/) (Figs. S3 and S4). The annual anthropogenic CO emissions in Africa are 12.2 Tg yr^{-1} for 2000 from the GEOS-Chem inventories, which is lower than 62.5 Tg yr^{-1} for 2008 from the HTAP2 inventories. The anthropogenic NOx emissions from the GEOS-Chem inventories are 2.27 Tg yr^{-1} for 2000, also lower than 4.53 Tg yr^{-1} for 2008 from the HTAP2 inventories. Although the anthropogenic emissions contribute less significantly to the ozone generation in Africa, these differences in emission inventories imply that African ozone simulated by GEOS-Chem is with some uncertainties.

To track the transport of ozone that is generated in Africa, we use the tagged ozone mode in GEOS-Chem, in which odd oxygen is tagged ($O_x = O_3 + NO_2 + 2NO_3 + 3N_2O_5 + HNO_3 + HNO_4 + PAN$

+ PMN + PPN, Fiore et al., 2002; Zhang et al., 2008). Since ozone accounts for most of O_x, we refer to ozone instead of O_x for clarity. To prepare for the tagged ozone simulation, we first run GEOS-Chem in the full chemistry mode to generate the daily ozone production rate and loss frequency. Then we run GEOS-Chem in the tagged ozone mode, using the archived ozone production rate and loss frequencies to differentiate ozone produced in different regions, tagged as different tracers. As shown in Fig. 1, the source region, Africa, is defined as the region of 35^oS-15^oN, 20^oW-55^oE and 15^oN-35^oN, 20^oW-30^oE. Therefore, ozone produced in Africa below tropopause from all natural and anthropogenic sources is tagged as a tracer. We further divided Africa into northern hemispheric Africa (NHAF) and southern hemispheric Africa (SHAF) separated by the equator and the tropospheric layers, the lower troposphere (LT, from the surface to 700 hPa), the middle troposphere (MT, 700-300 hPa), and the upper troposphere (UT, 300 hPa-tropopause) so to add six more tracers. The receptor region, Asia, is defined as the region of 5^oN-60^oN, 60^oE-145^oE. In the simulation for a year, both seasonal variation of chemistry and meteorology are considered.

To study the meteorological influence on the interannual variation in the transport of African ozone to Asia, the tagged ozone simulation is conducted for 20 years from January 1986 to December 2006 (using 1986 for model spin-up). As our purpose is focused on the influence on transport, we allow the meteorology to vary from year to year but fix the chemistry constantly, i.e., using the archived daily ozone production and loss data in one year, i. e. 2005, for the 20 year simulation. This treatment is similar to previous studies (Liu et al., 2005; Sekiya and Sudo, 2014). Note that meteorology affects both transport (a physical process) and chemistry while this treatment only considers the former.

Numerical approaches to exploring the source-receptor relationships include (1) tagged tracer simulations, (2) trajectory simulations, (3) perturbation simulations, and (4) inverse simulations (Zhu et al., 2017). Compared with the other approaches, the tagged trace simulation can track ozone effectively from different source regions and to separate the contributions of ozone from different source regions to

a receptor region and quantify each region's contribution. One issue with the tagged ozone simulation is the nonlinearity of chemistry. This nonlinearity can cause large differences between the full chemistry and the tagged ozone simulations. To test this nonlinearity, ozone concentrations between the full

220   chemistry and the tagged ozone simulations are compared at four ozonesonde sites in Africa and India (Fig. S5). The difference is found to generally within ±5%, suggesting that this approach works in these regions without large bias.

2.2 The validation of GEOS-Chem simulations

GEOS-Chem has been used widely in studying pollution transport (Bey et al., 2001b; Koumoutsaris et

225   al., 2008; Zhang et al., 2008; Liu et al., 2011; Wang et al., 2011; Ridder et al., 2012; Long et al., 2015; Jiang et al., 2016; Huang et al., 2017; Ikeda et al., 2017; Zhu et al., 2017a; Zhu et al., 2017b). Tropospheric ozone simulated by GEOS-Chem has been extensively validated using ozonesonde and satellite data, such as in North America (Zhang et al., 2008; Zhu et al., 2017b), Europe (Kim et al., 2015), East Asia (Wang et al., 2011; Zhu et al., 2017a; Zhu et al., 2017b), and other regions (Liu et al.,

230   2009). These validation practices have suggested reasonable agreements between the model simulations and ozone measurements. Forwe an enhanced confidence on the model performance, we compare the GEOS-Chem simulations with the ozonesonde data in Africa and India and with the satellite measurements from the Tropospheric Emission Spectrometer (TES) instrument. Three ozonesonde stations in Africa are selected for their long record, including Santa Cruz in North Africa (28.42^{o}N,

235   16.26^{o}W, 36 m), Nairobi in East Africa (1.27^{o}S, 36.8^{o}E, 1745 m), and Irene in South Africa (25.91^{o}S, 28.21^{o}E, 1524 m). These ozonesonde data have been used in studying tropospheric ozone in Africa widely (Clain et al., 2009; Thompson et al., 2012, 2014). In Asia, comparisons between GEOS-Chem simulations and ozonsonde observations have been made by Liu et al. (2002) and Zhu et al. (2017b) at stations over the Pacific Rim, which suggested that GEOS-Chem can generally capture the vertical and

240   seasonal variations of ozone concentrations in the region. We further compare the GEOS-Chem

simulations at three Indian sites, including New Delhi in northern India (28.3°N, 77.1°E, 273 m), Poona in western India (18.53°N, 73.85°E, 559 m), and Thiruvananthapuram in southern India (8.48°N, 76.95°E, 60 m). The ozonesonde data are acquired from the World Ozone and Ultraviolet Radiation Data Centre (WOUDC) (http://www.woudc.org/home.php) and the monthly TES product TL3O3M are from the NASA Langley Atmospheric Science Data Center. The monthly TES product TL3O3M (https://eosweb.larc.nasa.gov/project/tes/tes_table).

Fig. 2 shows the simulated and measured vertical ozone profiles by season, which are averaged from 1999 to 2003 at Santa Cruz, from 2003 to 2006 at Nairobi, and from 1999 to 2005 at Irene. Fig. 3 compares the time series of monthly ozone concentrations between the model simulations and ozonesonde measurements at different tropospheric layers at the sites. The corresponding bias, root-mean-square error (RMSE), and the correlation coefficient (r) between the two datasets are shown in Table 1 for the vertical profiles and in Table 2 for the time series, respectively

For the ozone vertical profiles (Fig. 2 and Table 1), GEOS-Chem appears to reasonably capture the ozone vertical variation and its seasonality at the three sites. It appears that GEOS-Chem overestimates ozone in the upper troposphere at Santa Cruz in NH winter and spring and underestimates ozone in the upper troposphere at Nairobi in NH summer and autumn. The correlation coefficients between the two data are above 0.9 for most seasons at the three sites. The mean biases ranges from -9.3% (at Nairobi in October) to 23.2% (at Santa Cruz in January), while the RMSE ranges from 4.3 ppbv (at Nairobi in April) to 15.5 ppbv (at Santa Cruz in January). The bias and RMSE suggest that the model performs no better at a station or a season than the other station or season.

For the time series of ozone at the upper, middle and lower troposphere, as well as the surface layer (Fig. 3 and Table 2), GEOS-Chem also performs reasonably well. The correlation coefficients between the two datasets in the tropospheric layers range within 0.57-0.79 at Santa Cruz, 0.76-0.90 at Nairobi, and 0.61-0.82 at Irene, all significant at a 95% significant level. The correlation coefficient is 0.60, 0.82,

265 and 0.39 for the surface layer at Santa Cruz, Nairobi, and Irene, respectively. However, the model underestimates upper tropospheric ozone in Nairobi (Table 2, Bias= -14.2%), somewhat overestimate ozone in 500- 300 hPa at Santa Cruz (Table 2, Bias= 4.5%) and near the surface at Irene (Table 2, Bias=60.3%). Generally, the model performs better in the lower and middle troposphere (RMSE ranges 3.5-12.7 ppbv) than in the upper troposphere (RMSE ranges 13.0-22.9 ppbv) at the three sites (Fig. 4).

270   The comparison between the GEOS-Chem and ozonesonde data at the three India sites is shown in a seasonal-altitude distribution in Fig. 5. The ozone concentrations are the means between 1994 and 2003. The time series of ozonesonde data at the sites are not shown because of inadequate records. Despite the seasonal-altitude patterns of ozone at the three sites are well simulated, the model overestimates the ozone near the surface and underestimates the ozone in the middle and upper troposphere at the three

275 sites. The annual mean bias at New Delhi is 5.6%, -14.5%, and -18.9% in the lower (LT), middle (MT), and upper (UT) troposphere, respectively. At Poona, it is 2.1%, -5.6%, and -19.1% in the LT, MT, and UT, respectively, while the annual mean bias at Thiruvananthapuram is -4.4% in the LT, -13.3% in the MT and -27.4% in the UT.

The global distribution of ozone from the GEOS-Chem simulations is compared with the TES

280 observation in 2005 in the four seasons at 464 hPa (Fig. S6), a layer around which the TES satellite data have the least bias. The GEOS-Chem simulations are smoothed with the TES averaging kernels and *a priori*. Generally, GEOS-Chem can capture the global variation of ozone in space and by season, such as high ozone over the NH middle latitudes in NH spring and summer and high ozone plumes from biomass burning over southern Africa in NH autumn. The smoothed ozone concentrations are generally

285 lower than the TES observation over Africa in all the seasons, about 20 ppbv (or 20%) in maximum. Note that TES ozone retrievals generally are higher than ozonesonde data, having a mean positive bias of 3-11 ppbv in the troposphere (Nassar et al., 2008).

Overall, GEOS-Chem can generally capture the seasonality of ozone profile in the ozonsonde data

over Africa. No systematic bias is suggested for a specific station, a season, or a tropospheric layer. In
290   Asia, GEOS-Chem tends to overestimate ozone in the lower troposphere and underestimate ozone in the
upper troposphere at three Indian sites, similar to what was documented in Liu et al. (2002) and Zhu et
al. (2017) for the Pacific Rim region. The GEOS-Chem simulations also compare reasonably with
satellite TES data in space and time.

2.3 The HYSPLIT trajectory model and meteorological data

295

We use HYSPLIT_4 (Hybrid Single-Particle Lagrangian Integrated Trajectory, version 4) (Draxler and
Hess, 1998; Stein et al., 2015) forward trajectory simulation to examine the transport pathways of
African ozone to Asia that further supplement the analysis from the GEOS-Chem simulations. The
HYSPLIT model is one of the most extensively used atmospheric transport and dispersion models
300   (Fleming et al., 2012). Meteorological inputs to HYSPLIT are the NCEP reanalysis at a resolution of
$2.5^o \times 2.5^o$ (http://ready.arl.noaa.gov/archives.php). Six-day forward trajectories are calculated from 1987
to 2006 four times a day (00, 06, 12 and 18 UTC) at seven African sites, including Cairo (31.1^oE, 30^oN),
Ghat (10.2^oE, 24.6^oN), Khartoum (32.3^oE, 15.4^oN), Abuja (7.3^oE, 9^oN), and Juba (31.4^oE, 4.5^oN) in
NHAF and Dar es Salaam (39.2^oE, 6.5^oS) and Luanda (13.1^oE, 8.5^oS) in SHAF. The locations of the
305   sites are shown in Fig. 1. The levels at 1.5 km, 5.5 km, and 11 km are selected to represent the lower,
middle, and the upper troposphere, respectively. The seven sites are chosen to represent two
longitudinal and 3-4 latitudinal zones in Africa.

The meteorological data include the NCEP/NCAR reanalysis I (Kalnay et al., 1996). The daily wind
fields are used to describe the climatology of atmospheric circulation during the study period from 1987
310   to 2006. The product is available on a $2.5^o \times 2.5^o$ horizontal grid at 17 pressure levels from 1000 hPa to
10 hPa (https://www.esrl.noaa.gov/psd/data/gridded/data.ncep.reanalysis.html).

Additionally, the monthly Outgoing Longwave Radiation (OLR) data from NCAR at $2.5^o \times 2.5^o$ with

temporal interpolation (Liebmann and Smith, 1996, https://www.esrl.noaa.gov/psd/data/gridded/data.interp_OLR .html) are used to indicate the intensity of the ITCZ. The dataset has been widely used

315   for tropical studies on deep convection and rainfall (Mounier and Janicot, 2004).

3 Seasonal variations of the transport of African ozone to Asia

3.1 Seasonal variations in African ozone over Asia

Because a substantial amount of ozone and ozone precursors are produced or emitted in Africa,

320   tropospheric ozone in the other continents is largely influenced by ozone outflow from Africa (Aghedo et al., 2007; Zare et al., 2014). Fig. 5 shows seasonal variations of imported African ozone in the Asian troposphere, varying with latitude and altitude. The values are the 20-year means (1987-2006) from the GEOS-Chem simulation. The largest African influences appear in the Asian middle and upper troposphere, i.e., 12-16 ppbv at 500 and 200 hPa. African ozone in the Asian lower troposphere is

325   reduced to 2-10 ppbv at 700 hPa throughout the year. Unlike imported European and North American ozone that influences Asia mostly over high altitudes, i.e., north of 30°N, (Zhu et al., 2017b), imported African ozone prevails over lower latitudes, generally from 5-40°N, considerably larger than European and North American ozone south of 30°N (Wild et al., 2004; Sudo and Akimoto, 2007; Zhu et al., 2017b). North of 50°N, African ozone influence is small, i.e., less than 8 ppbv and 2 ppbv, respectively,

330   above and below the Asian middle troposphere. Seasonally, imported African ozone in the upper troposphere peaks in NH spring around 30°N (~16 ppbv, Fig. 5a) and is at its minimum in NH summer south of 25°N. Owing to the high radiative forcing efficiency, the change in ozone concentrations in the upper troposphere can impact climate more significantly than that in the lower troposphere (Lacis et al., 1990). Therefore, the influence of African ozone on the climate in southern Asia is likely larger than

335   that of European and North American ozone. In the middle troposphere (Fig. 5b), African ozone is at the maximum (~16 ppbv) in NH winter between 20 ^{o}N and 25°N. In the lower troposphere (Fig. 5c),

between 5-40°N, African ozone is high in NH winter (~6-10 ppbv), while south of 10°N, African ozone has another peak in NH summer (~4 ppbv). Near the surface (Fig. 5d), African ozone concentrations are low, i.e. below 4 ppbv.

The strong seasonality of imported African ozone can also be shown vertically in Fig. 6a, in which imported African ozone is averaged over Asia south of 40°N. The fractional contribution of imported African ozone to ozone in Asia is shown in Fig. 6b. In the Asian upper troposphere, imported African ozone is largest during March-May (over 10 ppbv) and least during July-October (below 6 ppbv). In the Asia middle troposphere, imported African ozone is at a minimum from July to September (~4 ppbv, 6% in the fractional contribution) and a maximum (over 10 ppbv, 14% in the fractional contribution) from January to March, about one month earlier than in the upper troposphere. In the Asian lower troposphere, imported African ozone is largest in NH winter (~4 ppbv, 8% in the fractional contribution) and lowest in NH autumn (~2 ppbv, 5% in the fractional contribution).

Furthermore, the total imported African ozone over Asia is divided by tropospheric layer (UT, MT, and LT) and by hemisphere and the fractional contribution for each region is shown in Fig. 7. Over the Asian upper troposphere, African ozone from the NHAF UT accounts for 60-70% of the total imported African ozone (Fig. 7a), decreasing to ~20% in the Asian MT (Fig. 7b) and to below 20% in the Asian LT (Fig. 7c). In the meantime, the influence of African ozone from the NHAF MT becomes larger in the Asian MT and LT (20-40%). So does the influence of African ozone from the NHAF LT (20-40%). African ozone from SHAF contributes to the total imported ozone throughout the year in the three tropospheric layers. The contribution is small, usually below 20% of the total imported African ozone, except for in NH winter over the Asian UT (Fig. 7a) and in NH summer over the Asian LT (Fig. 7c). The two exceptions in interhemispheric transport will be discussed in detail in section 4

The seasonality of the transport of African ozone to Asia results from the collective impact of the emissions of ozone precursors in the source region and the meteorology and chemistry from the source

region to the receptor region. The precursors of African ozone are mainly from biogenic, biomass burning, and lightning NO_x sources (Piketh and Walton, 2004; Thompson, 2004; Aghedo et al., 2007; Giglio et al., 2013; Monks et al., 2015). The seasonality of emissions from biogenetic sources, biomass burning, lightning, and anthropogenic sources in Africa is characterized rather differently from the other

365   continents (Williams et al., 2009; Guenther et al., 2012; Giglio et al., 2013; Albrecht et al., 2016). Since Africa covers areas in both the hemispheres with a large portion in the tropics, the atmospheric circulation over Africa experiences obvious seasonal changes induced by the seasonality of the ITCZ and the Hadley cell (Nicholson, 2008, 2009; Žagar et al., 2011; Suzuki, 2011). To cast some light on the seasonal variations of imported African ozone over Asia presented in this section, the ITCZ and ozone

370   precursor emissions over Africa are discussed in section 3.2. Based on the discussion, the possible mechanisms that modulate the transport of African ozone to Asia are speculated in section 3.3.

3.2 ITCZ and ozone precursor emissions over Africa

Based on Nicholson (2009, 2013), Suzuki (2011), and Žagar et al. (2011), the mean positions of the

375   ITCZ in Africa in the four seasons are approximately illustrated in Figs. 9a-9d. The latitudinal migration of the ITCZ with season varies with longitude and the migration is within a wider range of latitudes in eastern Africa (10^oE-40^oE) than in western Africa (west of 10°E). In eastern Africa, ITCZ shifts between ~10^oS in NH winter and ~20^oN in NH summer, while in western Africa, the center of the ITCZ swings from 5^oN to 20^oN between NH winter and summer within the NH.

380   African ozone and its seasonality depend on biogenic, biomass burning, lightning and anthropogenic emissions. The anthropogenic emissions are generally considered to be small and have weak seasonality (Aghedo et al., 2007; Williams et al., 2009). Based on the emission inventories in GEOS-Chem that are described in section 2.1, the spatial distributions of ozone precursor emissions by season are shown in Fig. 8, including isoprene emissions from biogenic sources, CO emissions from biomass burning, and

385   NO_x emissions from lightning at 700 and 300 hPa. Seasonal variations of these emissions averaged over Africa, NHAF and SHAF are shown in Fig. 9.

    Isoprene (C_5H_8) is the dominant non-methane volatile organic compound (NMVOC) emitted by vegetation (Marais et al., 2012). Biogenic isoprene emissions in Africa are considered to be responsible for about 65% of ozone enhancement in the African upper troposphere (Aghedo et al., 2007). Isoprene

390   emissions shown in Figs.8a-8d are representative of biogenic emissions of ozone precursors. The magnitude and spatio-temporal pattern of the isoprene emissions in Africa are comparable with Marais et al. (2014). The maximum biogenic isoprene emissions are over central African rainforests throughout the year (Figs. 8a-8d). The seasonal cycle of biogenic isoprene over Africa peaks in NH spring and autumn (Fig. 9a). Plenty of non-methane VOCs are emitted from biogenic sources that can be uplifted

395   by strong convection. Aghedo et al. (2007) and Zare et al. (2014) suggested that biogenic emissions can lead to more ozone generation in the African upper troposphere than biomass burning and anthropogenic emissions.

    In NH winter, fires in Africa are active in the NH between 0-10°N and 15°W to 40°E (Fig. 8, 2nd row, also see Sauvage et al., 2005). From NH winter to autumn, biomass burning regions shift southward

400   (Fig. 8, 2nd row, also see van der Werf et al., 2010; Giglio et al., 2013). In NH summer, fires are most active in the SH from the equator to 20°S. Therefore, the regional CO emissions from biomass burning in NHAF peak during NH winter while in SHAF during NH summer (Fig. 9b). Aghedo et al. (2007) stated that biomass burning has the largest impact on surface ozone in the vicinity of the African burning regions during the burning seasons.

405   In Africa, lightning NO_x is produced mostly in the middle to upper troposphere (Figs. 8i-8p, also see Pickering et al., 1998; Ott et al., 2010; Miyazaki et al., 2014). Miyazaki et al. (2014) estimated that the altitudes where the annual lightning NO_x emissions maximize are around 11 km in northern Africa and 9.36 km in southern Africa. Aghedo et al. (2007) suggested that lightning emissions mainly enhance

ozone production in the African middle and upper troposphere. Ascribe to the high efficiency of deep

410   moist convection, frequent lightning activities occur in the ITCZ (Christian et al., 2003; Avila et al., 2010). Collier and Hughes (2011) suggested that the peak lightning activities are generally located on the southern border of the ITCZ in Africa. The seasonality of the locations for high lightning NO_x emission clearly shows the influence of the solar declination and the ITCZ over Africa (Collier and Hughes, 2011). When the ITCZ reaches to its northernmost position in NH summer (Fig. 8c), lightning

415   NO_x emission over NHAF becomes the highest (Figs. 9c and 9d). Similarly, the lightning NO_x emission over SHAF peaks in NH winter (Figs. 9c and 9d).

3.3 Analysis of the mechanisms for the transport of African ozone to Asia

As African ozone mainly peaks in the Asian middle and upper troposphere, the horizontal distributions

420   of African ozone at 400 hPa in January, April, July, and October overlaid with winds are shown in Fig. 10 to illustrate the seasonality and the transport pathways of African ozone to Asia at this level. In NH winter, African ozone can be transported for a long distance along the subtropical westerlies in the two hemispheres, reaching the western Pacific in the NH and across Australia in the SH, respectively. In NH summer, the NH subtropical westerlies and tropical easterlies shift to their northernmost positions; less

425   African ozone can be transported to Asia than in the other seasons. Furthermore, Fig. 11 shows the latitude-altitude cross sections of African ozone and winds averaged from 0 to 40^oE. This is to show how African ozone in the source region varies vertically along different latitudes. Fig. 12 is the same as Fig. 11 but for the longitude-altitude cross sections averaged from 20^oN to 35^oN so to show the transport pathway along longitude from Africa to Asia. Fig. 13 shows the 20-year mean paths for the

430   trajectories originated from seven reprehensive sites (Cairo, Ghat, Abuja, Khartoum, Juba, Dar es Salaam, and Luanda) and finally reach Asia. The mean paths are shown by season and by the original tropospheric layer, including the lapse day from the beginning of the trajectories. Additionally, we

conduct three sensitivity experiments by switching off the biogenic, lightning, and biomass burning emissions, respectively, to assist our analysis. The separate contributions of the three sources to

435   tropospheric ozone over Africa are shown in Fig. S7. In the following, we analyze the information from these figures, in combination with literature, to explore possible mechanisms responsible for the transport of African ozone to Asian in the four seasons

3.3.1 In NH winter

440   In NH winter, the eastern part of ITCZ shifts to its southernmost position in eastern Africa around 15°S (Figs. 8a and 11a), while the western part of the ITCZ remains in NHAF around 5°N (Figs. 8a and 11a). In Fig 11a, the ITCZ around the two latitudes and the two cells of the Hadley circulation are clearly shown. Biomass burning is active in NHAF (Figs. 8e and 9b) Biogenic emissions (Fig. 9a) and NO_x emissions from lightning are the highest in SHAF (Fig. 9c). All these conditions are well reflected in

445   Fig. 11a. The high African ozone concentration in the NHAF lower troposphere from the equator to 10^oN is resulted from high biomass burning and biogenic emissions (Figs. 8a and 8e, also see Figs. S7a and S7c, Aghedo et al., 2007), only the ozone is mostly confined under 700 hPa. In contrast, the high ozone concentrations over the SHAF middle and upper troposphere are due to deep convection and strong convergence of the ITCZ in SHAF that brings biogenic precursors to the upper troposphere and

450   enhance ozone production there (Fig. 8a, also see S9a). In addition, ozone can be also generated in the middle and upper troposphere due to frequent lightning activities (Fig. 8i, also see Fig. S9b, Aghedo et al., 2007).

Driven by the Hadley cell, African ozone is transported upward over the ITCZ, northward in the middle and upper troposphere, and equatorward in the lower troposphere. The northward flow in the

455   middle and upper troposphere gradually weakens between 15-30°N (Fig. 11a) where air parcels merge into the NH westerlies. This is also seen in the HYSPLIT trajectories in Figs. 13a and 13b. The trajectories originated from the two sites in the SH stop moving northward and shift eastwards instead around 20°N (Figs. 14a and 14b).

    From the source region to the receptor region, the NH subtropical westerlies build the pathways (Fig.
460   12a, also see trajectories in Figs. 13a and 13b). In Fig. 12a, along the latitudinal pathways, downdrafts behind the European trough around 40°E divert part of African ozone to the surface. However, the updrafts ahead of the European trough favor the uplift of African ozone so it can be transported for long distance in the upper troposphere.

    Finally, over the receptor region Asia, the downdrafts behind the Asian trough situated at around
465   140°E bring African ozone from the upper layers to the lower layers. Consequently, the contribution of African ozone to Asia becomes the highest in the middle and upper troposphere (Figs. 5 and 6). In NH winter, the transport of African ozone to Asia generally takes 4-6 days varying with altitude and latitude (Figs. 13a and 13b).

3.3.2 In NH spring

470   In NH spring, a region with high ozone concentrations above 40 ppbv appears in higher altitudes and extends to a larger area in the middle and upper troposphere than in NH winter (Figs. 11b and 12b). This region is further north than the high ozone region in NH winter. This is because the ITCZ in eastern Africa shifts northward to near the equator (Fig. 8b). Biomass burning is least active in both NHAF and SHAF (Figs 8f and 9b) while the biogenic emissions are the largest in NHAF and the second largest in
475   SHAF (Fig. 9a).As the ITCZ is over the region where biogenetic emissions are also high near the equator (Fig. 8b), The ITCZ effectively uplifts the biogenic precursors and also leads to production of

NO$_x$ from lightning in the upper layers (Fig.8j). The ozone precursors from both sources can enhance the generation of ozone in the middle and upper troposphere (Figs. S7d and S7e, also see Aghedo et al., 2007) where high ozone concentrations are apparent in Fig. 11b. Therefore, more African ozone can be exported out of Africa in the upper troposphere in NH spring than in NH winter (Fig.10a vs. 10b, Fig.12a vs. 12b. It takes more time for trajectories to arrive Asia in NH spring than in NH winter (Fig. 13a vs 13d).

3.3.3 In NH summer

In NH summer, the ITCZ in Africa swings to its northernmost position around 15°N (Figs.8c and11c).The region with active biomass burning shifts to SHAF (Figs. 8g and 9b). A large amount of ozone, generated from the biomass burning in SHAF, is shown in Fig. 11c over the SHAF lower troposphere from ~15°S to the equator. However, this ozone is mostly confined in the lower to the troposphere (Figs. 11c, S2i). Note that ozone in the middle and upper troposphere north of 15°N is higher than in the other seasons, which is likely resulted from lightning activities and biogenic emissions (Figs. 8k, S2h and S2g). This ozone can be readily transported to Asia.

Along the transport pathway Africa to Asia (Fig. 12c), Africa nozone concentrations at the source region are the highest among the four seasons (Figs. 10c and 12c). However, meteorological conditions along the pathway are most unfavorable for the transport of African ozone to Asia because of multiple reasons. First, the NH subtropical westerly jet in NH summer moves the northernmost position to around 40°N (Huang et al., 2012). The tropical easterlies also shift northward along (Fig. 8c) so to prevent African ozone from reaching Asia between 10°N and 30°N in the middle and upper troposphere (see Figs. 5 and 6 for imported African ozone concentrations, Figs. 10c and12c for wind fields). Second, on the transport pathway, the heavy downdrafts from the Saharan High, a midtropospheric

high-pressure system that is an eastward extension of the Azores High (Nicholson, 2017) and the

500   Arabian High in the middle troposphere over Middle East (Liu et al., 2011) hamper African ozone from

reaching Asia. Note in Fig. 12c, there is a region with lower African ozone than its surrounding in the

lower troposphere between 10°E and 40°E. The downwards of African ozone near 30°E is likely due to

a summertime trough at 40°E (Zhu et al., 2017b). Consequently, the amount of African ozone is reduced

during the transport. Thirdly, in the source region, strong updrafts occur over the Tibetan Plateau (Fig.

505   12c) and further block the transport of African ozone eastward. Finally, the strong divergence from the

South Asia High obstructs the eastward transport of African ozone in the upper troposphere. For these

reasons, imported African ozone over Asia is lower in NH summer than in the other seasons (Figs. 5 and

6). There are scarcely any trajectories from the African sites that can cross Asia like in the other seasons

(Figs. 13g, 13h, and 13i).

510

3.3.4 In NH autumn

In NH autumn, the ITCZ shifts southward to a location similar to in NH spring (Fig. 8b vs. 8d).

Biogenic emissions are slightly lower than in NH spring (Fig. 8b vs. 8d, Fig. 9a), whereas lightning

NO_x emissions are higher than in NH spring (Fig. 8j vs. 8l, Fig. 9c). Biomass burning is strong but

515   occurs mostly in SHAF (Fig. 8j vs. 8l, Fig.9b) so that it imposes small influence on the Asian

troposphere (Fig.7). In NHAF, the strong biogenic emissions are uplifted effectively by the ITCZ,

similar to NH spring. The uplifted biogenic precursors and NO_x from lightning in the middle and upper

troposphere lead to elevated ozone there (Fig. 11d, see also Figs. S7i and S7k). African ozone in the

NHAF middle and upper troposphere looks higher than in NH spring (Fig. 10b vs. 10d, Fig. 11b vs. 11d,

520   Fig. 12b vs. 12d). However, there is less African ozone arriving Asia in NH autumn than in NH spring

(Figs. 5 and 6). This may be due to two reasons. In NH spring, elevated African ozone in NHAF is located in higher altitudes than in NH autumn (Fig. 11b vs. 11d, Fig. 12b vs. 12d). This ozone can be more effectively transported to Asia by more speedy winds in the upper layers. The second reason is because of the weaker subtropical westerlies in NH autumn than in NH spring (Fig. 10b vs. 10d, Fig. 12b vs. 12d, also see Huang et al., 2012). The transport pathways and the time for the transport of African ozone to Asia in NH autumn are similar to in NH spring, as shown in the trajectories (Fig. 13).

4 Meteorological influences on the interannual variation of the transport of African ozone to Asia

4.1 The ITCZ and African ozone transport to Asia in NH winter

As discussed, the ITCZ can impact meteorology in Africa (Sultan and Janicot, 2000; Xie, 2004; Hu et al., 2007; Collier and Hughes, 2011; Suzuki, 2011). The deep convection along the ITCZ can carry ozone precursors from biogenic, biomass burning, and anthropogenic emissions to the upper layers from the surface. The ITCZ is also a zone with large lightning activities and thus can impact the seasonality of NO_x emission from lightning. The convective divergence in the upper troposphere over the ITCZ in Africa plays a significant role in output of African ozone and in the interhemispheric transport between SHAF and NHAF (Fig. 11 and see trajectories in Fig. 13).

To investigate the impact of ITCZ on the interannual variation of the transport of African ozone to Asia, we use the monthly Outgoing Longwave Radiation (OLR) data from NCAR at $2.5^o \times 2.5^o$ with temporal interpolation (Liebmann and Smith, 1996, https://www.esrl.noaa.gov/psd/data/gridded /data.interp_OLR.html) as a proxy to indicate the intensity of the ITCZ. According to Waliser et al. (1993) and Fukutomi and Yasunari (2013), the number of the grid points with OLR ≤ 260 W/m^2 in the region of 15^oW-45^oE, 20^oS-20^oN can indicate the intensity of the convection over the ITCZ in Africa.

We find that intensity of ITCZ in Africa is mostly related to imported African ozone over Asia in NH winter. Fig. 14 shows the time series of anomalies of imported African ozone averaged over Asia,

against the intensity of the ITCZ over Africa. The intensity of the ITCZ is normalized, i.e., the normalized value is equal to the original value minus the mean and then divided by the standard deviation in January from 1987 to 2006. The intensity of the ITCZ and anomalies of imported African ozone over Asia are with the correlation coefficient (r) of 0.61, 0.46, and 0.64 at the lower (975 hPa), middle (600 hPa), and upper (200 hPa) troposphere in Asia, respectively, all statistically significant at the 95% level ($p<0.05$).

Separating by the hemisphere, significant correlations are also found between the ITCZ and imported NHAF ozone in the entire troposphere in Asia (Fig. 14). The interhemispheric transport of ozone from SHAF to Asia also correlates with the intensity of ITCZ in Africa well, with r being 0.56 in the Asian upper troposphere (Fig. 14a). The interhemispheric transport to Asian middle and lower troposphere is little so their time series are not shown.

Overall, when the intensity of the African ITCZ is stronger, more ozone and ozone precursors are uplifted to the middle and upper troposphere and transported northward and then eastward to Asia by the NH subtropical westerlies. Additionally, driven by the enhanced convective divergence over the ITCZ, more ozone from SHAF is transported across the equator and to the NHAF upper troposphere. Consequently, African ozone increases in the Asian middle and upper troposphere. Meanwhile, carried by the downdrafts from the Asian winter monsoon (Zhu et al., 2017b), more ozone is transported to the surface in Asia.

4.2 Meteorology and the interhemispheric transport of ozone from SHAF to Asia

As shown in Fig. 7 and discussed in earlier sections, ozone generated in SHAF can be transported across the equator and eventually reach Asia. This is illustrated in more detail in Fig 15, showing seasonal-altitude variations of imported ozone from NHAF and SHAF over Asia and the fractional contributions of NHAF and SHAF ozone to the total imported African ozone. Ozone from NHAF

accounts for over 80% of the total imported African ozone in the Asian tropospheric column throughout

570   the year, except in the upper troposphere during NH winter and in the lower troposphere during NH

summer (Figs. 15b and 15d). This represents two important interhemispheric transport pathways.

For the first transport pathway, Fig. 7 suggests that the SHAF ozone originates mainly from the

SHAF UT. This ozone can be transported northward across the equator along the Hadley circulation and

then eastward to Asia by the NH subtropical westerlies (Fig. 13a). The amount of ozone being

575   transported is at the maximum in NH winter and at the minimum in NH summer (Figs. 7, and 15c)

when the ITCZ is at its southernmost and northernmost position, respectively (Fig. 8). This can be

further illustrated in the horizontal distribution of SHAF ozone at 200 hPa (Fig. 16a). SHAF ozone is 2-

4 ppbv over China south of 30°N and 4-6 ppbv over western India. As shown in section 4.1, the

variation of the ITCZ intensity in Africa can explain 31% the interannual variation of the transport of

580   SHAF ozone to the Asian upper troposphere in NH winter.

The second transport pathway is shown in Fig. 16b for SHAF ozone distribution at 850 hPa in July,

as Fig. 7c also suggests that the interhemispheric transport mainly occurs from the SHAF lower and

middle troposphere. SHAF ozone concentrations are 2-4 ppbv over the Arabian Sea and the west coast

of the Indian subcontinent. This ozone is transported to India in NH summer by the Somali cross-

585   equatorial flow (Fig. 16b), which is the strongest seasonal cross-equatorial flow in the lower

troposphere, serving as an essential component of the Asian monsoon system (Zhu, 2012). This is the

reason for the maximum SHAF ozone (~4 ppbv) over the Asian lower troposphere south of 10°N in NH

summer (Fig. 5c). One more evidence for this transport is shown in the trajectories from Dar es Salaam,

eastern coast of Africa (Figs. 13h and 13i). The interhemispheric ozone transport to western India takes

590   more than 6 days. Furthermore, the signal of the transport is captured in the ozonesonde data in western

India. The vertical distributions of the seasonal ozone at Poona and Thiruvananthapuram are shown for

the ozonsonde and GEOS-Chem data (Fig. 4). A dip of lower tropospheric ozone concentrations in both

data is apparent in NH summer, when the Somali jet carries clear air masses from sea which can be traced back to SHAF (Figs. 13h, 13i and 16b).

595   To search for a connection between the Somali jet and the imported SHAF ozone over western India, we use an index to indicate the intensity of the Somali jet that is proposed by Li et al. (2014a) The index is calculated as the mean meridional wind at 850 hPa in the domain shown in Fig. 17b. Li et al. (2014a) correlated the Somali jet and other cross-equatorial flows with the index. Fig. 18 shows the anomaly of SHAF ozone averaged in the lower troposphere at Poona and Thiruvananthapuram during NH summer

600   from 1987 to 2006. Positive correlations are found between the anomaly and the intensity of the Somali jet at both sites with the correlation coefficients over 0.56, significantly at the 95% level.

5 Discussion and conclusions

We have characterized the transport of African ozone to Asia according to the simulations of a global

605   chemical transport model, GEOS-Chem, for 20 years from 1987 to 2006. The ozone generated in the African troposphere is tracked using the tagged tracer simulation with GEOS-Chem. Combining with analysis of trajectory simulations using HYSPLIT and meteorological data of winds and OLR, we draw conclusions with discussion as follows.

1. In Asia, imported African ozone shows strong seasonality that varies greatly with latitude,

610   longitude, and altitude in the troposphere (Figs. 5 and 6). The influence of African ozone mainly prevails in Asia south of 40°N. From 5-40°N, imported African ozone is largest from March to May (10-16 ppbv) and lowest during July-October (2-6 ppbv) in the Asian upper troposphere (Fig. 5a). In the middle troposphere, imported African ozone is at a maximum from January to March (10-16 ppbv) and at a minimum from July to September (2-4 ppbv). Near the surface, the

615   African influence is small (below 6 ppbv). Overall, the influence of African ozone peaks in the Asian middle and upper troposphere between 20°N and 30°N in NH winter and spring. Over 5-

40°N, the mean fractional contribution of imported African ozone to the overall ozone concentrations in Asia is largest during NH winter in the middle troposphere (~18%) and lowest in NH summer throughout the tropospheric column (~6%).

2. Both the tagged ozone and the trajectory simulations show that the Hadley cell connects the subtropical westerlies to form a transport route from Africa to Asia (Figs. 10-13). This is a primary pathway that occurs throughout the year. It takes 4-6 days for African ozone to reach Asia depending on the season and the initial altitude and latitude of the airmass, i.e., faster in NH winter than in NH summer, faster in the upper troposphere than in the middle and lower troposphere, and faster in higher latitudes than in the lower latitudes (Fig. 13). The second transport pathway only appears in NH summer that runs from eastern Africa near the equator to the Indian low troposphere (Figs. 13h and 13i). It takes 6 or more days for African ozone to reach Asia along this pathway.

3. The seasonality of African ozone influence on Asia results from the collective effects of meteorology chemistry, and ozone precursor emissions in the source and receptor regions and between them. For the primary transport pathway, ozone and ozone precursors from various sources in Africa can be efficiently lifted up to high altitudes by the ITCZ. The African ozone in the middle and upper troposphere can be transported northward along the upper branch of the Hadley circulation and then eastward to Asia along the NH subtropical westerlies in the middle and upper troposphere. Therefore, the seasonal swings of the Hadley cell and NH subtropical westerlies play a dominant role in determining the seasonality of this transport pathway. Consequently, imported African ozone in Asia is least in NH summer, increasing toward both NH spring and NH autumn. In NH spring, there are more biogenic and lightning NO_x emissions than in NH winter. These precursors are uplifted by the ITCZ, making more ozone there than in NH winter. Consequently, there is more African ozone to be transported to the Asian upper

troposphere in NH spring than in winter (Fig. 5a and 6a). Although ozone appears higher in Africa in NH autumn than in spring, there is less imported African ozone over Asia in NH autumn than in spring (Fig. 5 and 6a), likely due to the facts that the NH subtropical westerlies are stronger in NH spring than in autumn and the elevated ozone in NHAF is located in higher altitudes in NH spring than in autumn. In NH summer, although the ozone outflow from Africa is high, it hardly reaches Asia because of the blockings of Saharan High, Arabian High, and Tibetan High along the transport pathway in the middle and upper troposphere, in addition to the northward swing of the westerlies. Finally, the ITCZ in Africa combining with the geographic variations in ozone precursor emissions with season can also modulate the seasonality of transport of African ozone to Asia. When the ITCZ coincides with the ozone precursor emissions from biogenic and biomass burning emissions, in addition to enhanced NO_x emissions from lightning, strong ozone export out of Africa can be resulted, such as in NH spring.

4. The interannual variation of the transport of African ozone to Asia is closely related to the intensity of the ITCZ in Africa in NH winter. Positive correlations are found between the intensity of the ITCZ in Africa and imported African ozone over Asia ($r = 0.64$ at 200 hPa, $r = 0.46$ at 600 hPa, and $r = 0.61$ at 975 hPa, and p<0.05 for the three layers) (Fig. 14). The stronger the ITCZ in a NH winter is, the more ozone and its precursors from the surface emissions can be uplifted. In the meantime, more lightning NO_x is produced. Furthermore, the interhemispheric transport of ozone from SHAF is enhanced. Consequently, more African ozone can be transported to Asia.

5. Ozone from NHAF makes up over 80% of the total imported African ozone in the Asian troposphere in all layers and seasons, but with two exceptions in which ozone from SHAF becomes larger than 25% of the total imported ozone (Figs. 7 and 15). The first exception occurs in the Asian upper troposphere during NH winter, corresponding to the primary transport pathway in NH winter (Fig. 7). In the season, the ITCZ swings to its southernmost position in Africa and

665   the convective divergence over the ITCZ in the upper troposphere is enhanced, resulting in more interhemispheric transport of ozone from SHAF. The interhemispheric transport along this pathway is largest in NH winter and least in NH summer (Figs. 7 and15). The second exception takes place in the Asian lower troposphere during NH summer. The SHAF ozone is transported along the Somali jet, which is the second transport pathway, from eastern Africa near the equator

670   to India (Fig. 16), forming an African ozone maximum in the lower troposphere from the tropics to 15°N in NH summer (Fig. 5c). We find that the intensities of the ITCZ in Africa and the Somali jet can respectively explain approximately ~30% of the interannual variations in the transport of ozone from the southern hemispheric Africa to Asia in the two cases.

     This study provides an enhanced understanding of the source-receptor relationship of ozone transport

675   from Africa to Asia. The findings on the transport routes from this study may also be applicable to other atmospheric pollutants with similar lifetimes, such as carbon monoxide. Our analysis is based on the simulations from the GEOS-Chem and HYSPLIT models, both of which have their own biases associated with emission inventories, parameterization schemes, and input data. The influences of African ozone can be further assessed by separating different emission sources.

680

References

Aghedo, A. M., Schultz, M. G., and Rast, S.: The influence of African air pollution on regional and

695 global tropospheric ozone, Atmos. Chem. Phys., 7, 1193-1212, doi:10.5194/acp-7-1193-2007, 2007.

Akritidis, D., Pozzer, A., Zanis, P., Tyrlis, E., Škerlak, B., Sprenger, M., and Lelieveld, J.: On the role of

tropopause folds in summertime tropospheric ozone over the eastern Mediterranean and the Middle

East, Atmos. Chem. Phys., 16, 14025-14039, doi:10.5194/acp-16-14025-2016, 2016.

Albrecht, R. I., Goodman, S. J., Buechler, D. E., Blakeslee, R. J., and Christian, H. J.: Where are the

700 lightning hotspots on Earth?, Bull. Amer. Meteor. Soc., 97, 2051-2068, doi:10.1175/BAMS-D-14-

00193.1, 2016.

Allen, D., Pickering, K., Duncan, B., and Damon, M.: Impact of lightning NO emissions on North

American photochemistry as determined using the Global Modeling Initiative (GMI) model, J.

Geophys. Res., 115, D22301, doi:10.1029/2010JD014062, 2010.

705 Anenberg, S. C., Horowitz, L. W., Tong, D. Q., and West, J. J.: An estimate of the global burden of

anthropogenic ozone and fine particulate matter on premature human mortality using atmospheric

modeling, Environ. Health. Persp., 118, 1189-1195, doi:10.1289/ehp.0901220, 2010.

Avery, M., Westberg, D., Fuelberg, H., Newell, R., Anderson, B., Vay, S., Sachse, G., and Blake, D.:

Chemical transport across the ITCZ in the central Pacific during an El Nino-Southern Oscillation

710 cold phase event in March-April 1999, J. Geophys. Res., 106, 32539-32553,

doi:10.1029/2001JD000728, 2001.

Avila, E. E., Bürgesser, R. E., Castellano, N. E., Collier, A. B., Compagnucci, R. H., and Hughes, A. R.:

Correlations between deep convection and lightning activity on a global scale, J. Atmos. Sol-Terr. Phy., 72, 1114-1121, doi:10.1016/j.jastp.2010.07.019, 2010.

715 Bey, I., Jacob, D. J., Logan, J. A., and Yantosca, R. M.: Asian chemical outflow to the Pacific in spring: Origins, pathways, and budgets, J. Geophys. Res., 106, 23073-23095, doi:10.1029/2001jd000807, 2001a.

Bey, I., Jacob, D. J., Yantosca, R. M., Logan, J. A., Field, B. D., Fiore, A. M., Li, Q., Liu, H. Y., Mickley, L. J., and Schultz, M. G.: Global modeling of tropospheric chemistry with assimilated

720 meteorology: Model description and evaluation, J. Geophys. Res., 106, 23073-23095, doi:10.1029/2001jd000806, 2001b.

Bouarar, I., Law, K. S., Pham, M., Liousse, C., Schlager, H., Hamburger, T., Reeves, C., Cammas, J.-P., Nédéléc, P., and Szopa, S.: Emission sources contributing to tropospheric ozone over Equatorial Africa during the summer monsoon, Atmos. Chem. Phys., 11, 13395-13419, doi:10.5194/acp-11-

725 13395-2011, 2011.

Chakraborty, T., Beig, G., Dentener, F. J., and Wild, O.: Atmospheric transport of ozone between Southern and Eastern Asia, Sci. Total Environ., 523, 28-39, doi:10.1016/j.scitotenv.2015.03.066, 2015.

Choi, H. D., Liu, H., Crawford, J. H., Considine, D. B., Allen, D. J., Duncan, B. N., Horowitz, L. W.,

730 Rodriguez, J. M., Strahan, S. E., Zhang, L., Liu, X., Damon, M. R., and Steenrod, S. D.: Global O3–CO correlations in a chemistry and transport model during July–August: evaluation with TES satellite observations and sensitivity to input meteorological data and emissions, Atmos. Chem. Phys., 17, 8429-8452, doi:10.5194/acp-17-8429-2017, 2017.

Christian, H. J., Blakeslee, R. J., Boccippio, D. J., Boeck, W. L., Buechler, D. E., Driscoll, K. T.,

735 Goodman, S. J., Hall, J. M., Koshak, W. J., and Mach, D. M.: Global frequency and distribution of lightning as observed from space by the Optical Transient Detector, J. Geophys. Res., 108, ACL 4-1-

ACL 4-15, doi:10.1029/2002JD002347, 2003.

Clain, G., Baray, J. L., Delmas, R., Diab, R., Bellevue, J. L. D., Keckhut, P., Posny, F., Metzger, J. M., and Cammas, J. P.: Tropospheric ozone climatology at two Southern Hemisphere tropical/subtropical sites, (Reunion Island and Irene, South Africa) from ozonesondes, LIDAR, and in situ aircraft measurements, Atmos. Chem. Phys., 9, 1723-1734, doi:10.5194/acp-9-1723-2009, 2009.

Collier, A. B., and Hughes, A. R.: Lightning and the African ITCZ, J. Atmos. Sol-Terr. Phy., 73, 2392-2398, doi:10.1016/j.jastp.2011.08.010, 2011.

Cooper, O., Moody, J., Parrish, D., Trainer, M., Ryerson, T., Holloway, J., Hübler, G., Fehsenfeld, F., and Evans, M.: Trace gas composition of midlatitude cyclones over the western North Atlantic Ocean: A conceptual model, J. Geophys. Res., 107, 5-24, doi:10.1029/2001jd000901, 2002.

Cooper, O., Parrish, D., Stohl, A., Trainer, M., Nédélec, P., Thouret, V., Cammas, J.-P., Oltmans, S., Johnson, B., and Tarasick, D.: Increasing springtime ozone mixing ratios in the free troposphere over western North America, Nature, 463, 344-348, doi:10.1038/nature08708, 2010.

Cooper, O., Oltmans, S., Johnson, B., Brioude, J., Angevine, W., Trainer, M., Parrish, D., Ryerson, T., Pollack, I., and Cullis, P.: Measurement of western US baseline ozone from the surface to the tropopause and assessment of downwind impact regions, J. Geophys. Res., 116, 898-908, doi:10.1029/2011JD016095, 2011.

Cooper, O. R., Langford, A. O., Parrish, D. D., and Fahey, D. W.: Challenges of a lowered US ozone standard, Science, 348, 1096-1097, doi:10.1126/science.aaa5748, 2015.

Derwent, R. G., Utembe, S. R., Jenkin, M. E., and Shallcross, D. E.: Tropospheric ozone production regions and the intercontinental origins of surface ozone over Europe, Atmos. Environ., 112, 216-224, doi:10.1016/j.atmosenv.2015.04.049, 2015.

Doherty, O. M., Riemer, N., and Hameed, S.: Control of Saharan mineral dust transport to Barbados in winter by the Intertropical Convergence Zone over West Africa, J. Geophys. Res., 117, 161-169,

doi:10.1029/2012JD017767, 2012.

Doherty, O. M., Riemer, N., and Hameed, S.: Role of the convergence zone over West Africa in controlling Saharan mineral dust load and transport in the boreal summer, Tellus B, 66, 759-763, doi:10.3402/tellusb.v66.23191, 2014.

765   Doherty, R., Wild, O., Shindell, D., Zeng, G., MacKenzie, I., Collins, W., Fiore, A. M., Stevenson, D., Dentener, F., and Schultz, M.: Impacts of climate change on surface ozone and intercontinental ozone pollution: A multi-model study, J. Geophys. Res., 118, 3744-3763, doi:10.1002/jgrd.50266, 2013.

Doherty, R. M.: Atmospheric chemistry: Ozone pollution from near and far, Nat. Geosci., 8, 664-665, doi:10.1038/ngeo2497, 2015.

770   Doherty, R. M., Orbe, C., Zeng, G., Plummer, D. A., Prather, M. J., Wild, O., Lin, M., Shindell, D. T., and Mackenzie, I. A.: Multi-model impacts of climate change on pollution transport from global emission source regions, Atmos. Chem. Phys., 17, 14219-14237, doi:10.5194/acp-17-14219-2017, 2017.

Draxler, R. R., and Hess, G.: An overview of the HYSPLIT_4 modelling system for trajectories, Aust.

775   Meteorol. Mag., 47, 295-308, 1998.

Fiore, A. M., Jacob, D. J., Bey, I., Yantosca, R. M., Field, B. D., Fusco, A. C., and Wilkinson, J. G.: Background ozone over the United States in summer: Origin, trend, and contribution to pollution episodes, J. Geophys. Res., 107, ACH 11-1-ACH 11-25, doi:10.1029/2001JD000982, 2002.

Fiore, A. M., Dentener, F., Wild, O., Cuvelier, C., Schultz, M., Hess, P., Textor, C., Schulz, M., Doherty,

780   R., and Horowitz, L.: Multimodel estimates of intercontinental source-receptor relationships for ozone pollution, J. Geophys. Res., 114, 83-84, doi:10.1029/2008JD010816, 2009.

Fleming, Z. L., Monks, P. S., and Manning, A. J.: Review: Untangling the influence of air-mass history in interpreting observed atmospheric composition, Atmos. Res., 104, 1-39, doi:10.1016/j.atmosres.2011.09.009, 2012.

785   Fukutomi, Y., and Yasunari, T.: Structure and characteristics of submonthly-scale waves along the

Indian Ocean ITCZ, Clim. Dynam., 40, 1819-1839, doi:10.1007/s00382-012-1417-x, 2013.

Fukutomi, Y., and Yasunari, T.: Extratropical forcing of tropical wave disturbances along the Indian

Ocean ITCZ, J. Geophys. Res., 119, 1154-1171, doi:10.1002/2013JD020696, 2014.

Galmarini, S., Koffi, B., Solazzo, E., Keating, T., Hogrefe, C., Schulz, M., Benedictow, A., Griesfeller,

790   J. J., Janssens-Maenhout, G., Carmichael, G., Fu, J., and Dentener, F.: Technical note: Coordination

and harmonization of the multi-scale, multi-model activities HTAP2, AQMEII3, and MICS-Asia3:

simulations, emission inventories, boundary conditions, and model output formats, Atmos. Chem.

Phys., 17, 1543-1555, doi:10.5194/acp-17-1543-2017, 2017.

Garny, H., and Randel, W. J.: Transport pathways from the Asian monsoon anticyclone to the

795   stratosphere, Atmos. Chem. Phys., 16, 2703-2718, doi:10.5194/acp-16-2703-2016, 2016.

Giglio, L., Randerson, J. T., and Werf, G. R.: Analysis of daily, monthly, and annual burned area using

the fourth-generation global fire emissions database (GFED4), J. Geophys. Res., 118, 317-328,

doi:10.1002/jgrg.20042, 2013.

Guenther, A., Jiang, X., Heald, C., Sakulyanontvittaya, T., Duhl, T., Emmons, L., and Wang, X.: The

800   Model of Emissions of Gases and Aerosols from Nature version 2.1 (MEGAN2.1): an extended and

updated framework for modeling biogenic emissions, Geosci. Model Dev., 5, 1471-1492,

doi:10.5194/gmd-5-1471-2012, 2012.

Guerova, G., Bey, I., Attié, J.-L., Martin, R., Cui, J., and Sprenger, M.: Impact of transatlantic transport

episodes on summertime ozone in Europe, Atmos. Chem. Phys., 6, 2057-2072, doi:10.5194/acp-6-

805   2057-2006, 2006.

Hack, J. J.: Parameterization of moist convection in the National Center for Atmospheric Research

community climate model (CCM2), J. Geophys. Res., 99, 5551-5568, doi:10.1029/93jd03478, 1994.

Hartley, D. E., and Black, R. X.: Mechanistic analysis of interhemispheric transport, Geophys. Res.

Lett., 22, 2945-2948, doi:10.1029/95gl02823, 1995.

810   Hollaway, M. J., Arnold, S., Challinor, A. J., and Emberson, L.: Intercontinental trans-boundary

contributions to ozone-induced crop yield losses in the Northern Hemisphere, Biogeosciences, 9,

271-292, doi:10.5194/bg-9-271-2012, 2012.

Holloway, T., Sakurai, T., Han, Z., Ehlers, S., Spak, S. N., Horowitz, L. W., Carmichael, G. R., Streets,

D. G., Hozumi, Y., and Ueda, H.: MICS-Asia II: Impact of global emissions on regional air quality in

815   Asia, Atmos. Environ., 42, 3543-3561, doi:10.1016/j.atmosenv.2007.10.022, 2008.

HTAP: Hemispheric transport of air pollution 2010, United Nations, Dentener, F., Keating, T. and

Akimoto, H. (eds.), New York and Geneva, 2010.

Hu, Y., Li, D., and Liu, J.: Abrupt seasonal variation of the ITCZ and the Hadley circulation, Geophys.

Res. Lett., 34, 5407-5413, doi:10.1029/2007GL030950, 2007.

820   Huang, R., Chen, J., Wang, L., and Lin, Z.: Characteristics, processes, and causes of the spatio-temporal

variabilities of the East Asian monsoon system, Adv. Atmos. Sci., 29, 910-942, doi: 10.1007/s00376-

012-2015-x, 2012.

Huang, M., Carmichael, G. R., Pierce, R. B., Jo, D. S., Park, R. J., Flemming, J., Emmons, L. K.,

Bowman, K. W., Henze, D. K., Davila, Y., Sudo, K., Jonson, J. E., Tronstad Lund, M., Janssens-

825   Maenhout, G., Dentener, F. J., Keating, T. J., Oetjen, H., and Payne, V. H.: Impact of intercontinental

pollution transport on North American ozone air pollution: an HTAP phase 2 multi-model study,

Atmos. Chem. Phys., 17, 5721-5750, doi:10.5194/acp-17-5721-2017, 2017.

Huntrieser, H., Heland, J., Schlager, H., Forster, C., Stohl, A., Aufmhoff, H., Arnold, F., Scheel, H.,

Campana, M., and Gilge, S.: Intercontinental air pollution transport from North America to Europe:

830   Experimental evidence from airborne measurements and surface observations, J. Geophys. Res., 110,

372-384, doi:10.1029/2004JD005045, 2005.

Ikeda, K., Tanimoto, H., Sugita, T., Akiyoshi, H., Kanaya, Y., Zhu, C., and Taketani, F.: Tagged tracer

simulations of black carbon in the Arctic: transport, source contributions, and budget, Atmos. Chem. Phys., 17, 10515-10533, doi:10.5194/acp-17-10515-2017, 2017.

835   Jaffe, D., McKendry, I., Anderson, T., and Price, H.: Six 'new' episodes of trans-Pacific transport of air pollutants, Atmos. Environ., 37, 391-404, doi:10.1016/s1352-2310(02)00862-2, 2003.

Jiang, Z., Miyazaki, K., Worden, J. R., Liu, J. J., Jones, D. B. A., and Henze, D. K.: Impacts of anthropogenic and natural sources on free tropospheric ozone over the Middle East, Atmos. Chem. Phys., 16, 6537-6546, doi:10.5194/acp-16-6537-2016, 2016.

840   Kalnay, E., Kanamitsu, M., Kistler, R., Collins, W., Deaven, D., Gandin, L., Iredell, M., Saha, S., White, G., and Woollen, J.: The NCEP/NCAR 40-year reanalysis project, Bull. Amer. Meteor. Soc., 77, 437-471, doi:10.1175/1520-0477(1996)077<0437:tnyrp>2.0.co;2, 1996.

Karamchandani, P., Long, Y., Pirovano, G., Balzarini, A., and Yarwood, G.: Source-sector contributions to European ozone and fine PM in 2010 using AQMEII modeling data, Atmos. Chem. Phys., 17,

845   5643-5664, doi:10.5194/acp-17-5643-2017, 2017.

Kim, M. J., Park, R. J., Ho, C.-H., Woo, J.-H., Choi, K.-C., Song, C.-K., and Lee, J.-B.: Future ozone and oxidants change under the RCP scenarios, Atmos. Environ., 101, 103-115, doi:10.1016/j.atmosenv.2014.11.016, 2015.

Knowland, K. E., Doherty, R. M., Hodges, K. I., and Ott, L. E.: The influence of mid-latitude cyclones

850   on European background surface ozone, Atmos. Chem. Phys., 17, 12421-12447, doi:10.5194/acp-17-12421-2017, 2017.

Koumoutsaris, S., Bey, I., Generoso, S., and Thouret, V.: Influence of El Niño-Southern Oscillation on the interannual variability of tropospheric ozone in the northern midlatitudes, J. Geophys. Res., 113, D19301, doi:10.1029/2007JD009753, 2008.

855   Kuhns, H., Green, M., and Etyemezian, V.: Big Bend Regional Aerosol and Visibility Observational (BRAVO) Study Emissions Inventory, 2003.

Lacis, A. A., Wuebbles, D. J., and Logan, J. A.: Radiative forcing of climate by changes in the vertical distribution of ozone, J. Geophys. Res., 95, 9971-9981, doi:10.1029/jd095id07p09971, 1990.

Lal, S., Venkataramani, S., Chandra, N., Cooper, O. R., Brioude, J., and Naja, M.: Transport effects on the vertical distribution of tropospheric ozone over western India, J. Geophys. Res., 119, 10012-10026, doi:10.1002/2014JD021854, 2014.

Lefohn, A. S., Malley, C. S., Simon, H., Wells, B., Xu, X., Zhang, L., and Wang, T.: Responses of human health and vegetation exposure metrics to changes in ozone concentration distributions in the European Union, United States, and China, Atmos. Environ., 152, 123-145, doi:10.1016/j.atmosenv.2016.12.025, 2017.

Lelieveld, J., and Dentener, F. J.: What controls tropospheric ozone?, J. Geophys. Res., 105, 3531-3551, doi:10.1029/1999jd901011, 2000.

Lewis, A., Evans, M., Methven, J., Watson, N., Lee, J., Hopkins, J., Purvis, R., Arnold, S., McQuaid, J., and Whalley, L.: Chemical composition observed over the mid-Atlantic and the detection of pollution signatures far from source regions, J. Geophys. Res., 112, 815-838, doi:10.1029/2006JD007584, 2007.

Li, C., and Li, S.: Interannual Seesaw between the Somali and the Australian Cross-Equatorial Flows and its Connection to the East Asian Summer Monsoon, J. Climate, 27, 3966-3981, doi:10.1175/JCLI-D-13-00288.1, 2014a.

Li, X., Liu, J., Mauzerall, D. L., Emmons, L. K., Walters, S., Horowitz, L. W., and Tao, S.: Effects of trans-Eurasian transport of air pollutants on surface ozone concentrations over Western China, J. Geophys. Res., 119, 12338-12354, doi:10.1002/2014jd021936, 2014b.

Liebmann, B., and Smith, C. A.: Description of a complete (interpolated) outgoing longwave radiation dataset, Bull. Amer. Meteor. Soc., 77, 1275-1277, 1996.

Lin, M., Horowitz, L. W., Payton, R., Fiore, A. M., and Tonnesen, G.: US surface ozone trends and

extremes from 1980 to 2014: quantifying the roles of rising Asian emissions, domestic controls, wildfires, and climate, Atmos. Chem. Phys., 17, 2943-2970, doi:10.5194/acp-17-2943-2017, 2017.

Liu, H., Jacob, D. J., Chan, L. Y., Oltmans, S. J., Bey, I., Yantosca, R. M., Harris, J. M., Duncan, B. N., and Martin, R. V.: Sources of tropospheric ozone along the Asian Pacific Rim: An analysis of CO in the tropical troposphere using Aura satellite data and the GEOS-Chem model: ozonesonde observations, J. Geophys. Res., 107, ACH 3-1-ACH 3-19, doi:10.1029/2001JD002005, 2002.

Liu, J., Mauzerall, D. L., and Horowitz, L. W.: Analysis of seasonal and interannual variability of transpacific transport, J. Geophys. Res.,110, D04302, doi:10.1029/2004JD005207, 2005.

Liu, J., Logan, J. A., Jones, D. B. A., Livesey, N. J., Megretskaia, I., Carouge, C., and Nedelec, P.: insights into transport characteristics of the GEOS meteorological products, Atmos. Chem. Phys., 10, 12207-12232, doi:10.5194/acp-10-12207-2010, 2010.

Liu, J. J., Jones, D., Worden, J. R., Noone, D., Parrington, M., and Kar, J.: Analysis of the summertime buildup of tropospheric ozone abundances over the Middle East and North Africa as observed by the Tropospheric Emission Spectrometer instrument, J. Geophys. Res., 114, 730-734, doi:10.1029/2008JD010993, 2009.

Liu, J. J., Jones, D., Zhang, S., and Kar, J.: Influence of interannual variations in transport on summertime abundances of ozone over the Middle East, J. Geophys. Res., 116, 999-1010, doi:10.1029/2011JD016188, 2011.

Long, M., Yantosca, R., Nielsen, J., Keller, C., da Silva, A., Sulprizio, M., Pawson, S., and Jacob, D.: Development of a grid-independent GEOS-Chem chemical transport model (v9-02) as an atmospheric chemistry module for Earth system models, Geosci. Model. Dev., 8, 595-602, doi:10.5194/gmd-8-595-2015, 2015.

Marais, E. A., Jacob, D. J., Kurosu, T. P., Chance, K., Murphy, J. G., Reeves, C., Mills, G., Casadio, S., Millet, D. B., Barkley, M. P., Paulot, F., and Mao, J.: Isoprene emissions in Africa inferred from OMI

905   observations of formaldehyde columns, Atmos. Chem. Phys., 12, 6219-6235, doi:10.5194/acp-12-6219-2012, 2012.

Marais, E. A., Jacob, D. J., Guenther, A., Chance, K., Kurosu, T. P., Murphy, J. G., Reeves, C. E., and Pye, H. O. T.: Improved model of isoprene emissions in Africa using Ozone Monitoring Instrument (OMI) satellite observations of formaldehyde: implications for oxidants and particulate matter,

910   Atmos. Chem. Phys., 14, 7693-7703, doi:10.5194/acp-14-7693-2014, 2014.

Martin, R. V., Sauvage, B., Folkins, I., Sioris, C. E., Boone, C., Bernath, P., and Ziemke, J.: Space-based constraints on the production of nitric oxide by lightning, J. Geophys. Res., 112, D09309, doi:10.1029/2006JD007831, 2007.

Miyazaki, K., Eskes, H., Sudo, K., and Zhang, C.: Global lightning NO x production estimated by an

915   assimilation of multiple satellite data sets, Atmos. Chem. Phys., 14, 3277-3305, doi:10.5194/acp-14-3277-2014, 2014.

Monks, P. S., Archibald, A., Colette, A., Cooper, O., Coyle, M., Derwent, R., Fowler, D., Granier, C., Law, K. S., and Mills, G.: Tropospheric ozone and its precursors from the urban to the global scale from air quality to short-lived climate forcer, Atmos. Chem. Phys., 15, 8889-8973, doi:10.5194/acp-

920   15-8889-2015, 2015.

Mounier, F., and Janicot, S.: Evidence of two independent modes of convection at intraseasonal timescale in the West African summer monsoon, Geophys. Res. Lett., 31, 2876-2877, doi:10.1029/2004GL020665, 2004.

Myhre, G., Shindell, D., Bréon, F.-M., Collins, W., Fuglestvedt, J., Huang, J., Koch, D., Lamarque, J.-F.,

925   Lee, D., Mendoza, B., Nakajima, T., Robock, A., Stephens, G., Takemura, T., and Zhang, H.: Anthropogenic and Natural Radiative Forcing, In: Climate Change 2013: The Physical Science Basis, Contribution of Working Group I to the Fifth Assessment Report of the Intergovernmental Panel on Climate Change, Cambridge University Press, Cambridge, United Kingdom and New York, NY,

USA, 659-740, 2013.

930   Nagashima, T., Ohara, T., Sudo, K., and Akimoto, H.: The relative importance of various source regions on East Asian surface ozone, Atmos. Chem. Phys., 10, 11305-11322, doi:10.5194/acp-10-11305-2010, 2010.

Nassar, R., Logan, J. A., Worden, H. M., Megretskaia, I. A., Bowman, K. W., Osterman, G. B., Thompson, A. M., Tarasick, D. W., Austin, S., Claude, H., Dubey, M. K., Hocking, W. K., Johnson,

935   B. J., Joseph, E., Merrill, J., Morris, G. A., Newchurch, M., Oltmans, S. J., Posny, F., Schmidlin, F. J., Vömel, H., Whiteman, D. N., and Witte, J. C.: Validation of Tropospheric Emission Spectrometer (TES) nadir ozone profiles using ozonesonde measurements, J. Geophys. Res., 113, D15S17, doi:10.1029/2007JD008819, 2008.

Neu, J. L., Flury, T., Manney, G. L., Santee, M. L., Livesey, N. J., and Worden, J.: Tropospheric ozone

940   variations governed by changes in stratospheric circulation, Nat. Geosci., 7, 340-344, doi:10.1038/NGEO2138, 2014.

Nicholson, S. E.: The intensity, location and structure of the tropical rainbelt over west Africa as factors in interannual variability, Int. J.Climatol., 28, 1775-1785, doi:10.1002/joc.1507, 2008.

Nicholson, S. E.: A revised picture of the structure of the "monsoon" and land ITCZ over West Africa,

945   Clim. Dynam., 32, 1155-1171, doi:10.1007/s00382-008-0514-3, 2009.

Nicholson, S. E.: The West African Sahel: A Review of Recent Studies on the Rainfall Regime and Its Interannual Variability, ISRN Meteorology, 2013, 32, doi:10.1155/2013/453521, 2013.

Nicholson, S. E.: Climate and climatic variability of rainfall over eastern Africa, Rev. Geophys., 55, 590-635, doi:10.1002/2016RG000544, 2017.

950   Nopmongcol, U., Liu, Z., Stoeckenius, T., and Yarwood, G.: Modeling intercontinental transport of ozone in North America with CAMx for the Air Quality Model Evaluation International Initiative (AQMEII) Phase 3, Atmos. Chem. Phys., 17, 9931-9943, doi:10.5194/acp-17-9931-2017,

2017.

Olivier, J.G.J. and J.J.M. Berdowski, Global emissions sources and sinks. In: Berdowski, J., Guicherit, R. and B.J. Heij (eds.) The Climate System, pp. 33-78. A. A. Balkema Publishers/Swets & Zeitlinger Publishers, Lisse, The Netherlands., 2001

Ott, L. E., Pickering, K. E., Stenchikov, G. L., Allen, D. J., Decaria, A. J., Ridley, B., Lin, R. F., Lang, S., and Tao, W. K.: Production of lightning NOx and its vertical distribution calculated from three-dimensional cloud-scale chemical transport model simulations, J. Geophys. Res., 115, 288-303, doi:10.1029/2009JD011880, 2010.

Philip, S., Martin, R. V., and Keller, C. A.: Sensitivity of chemistry-transport model simulations to the duration of chemical and transport operators: a case study with GEOS-Chem v10-01, Geosci. Model. Dev., 9, 1683-1695, doi:10.5194/gmd-9-1683-2016, 2016.

Pickering, K. E., Wang, Y., Tao, W. K., Price, C., and Müller, J. F.: Vertical distributions of lightning NOx for use in regional and global chemical transport models, J. Geophys. Res., 103, 31203-31216, doi:10.1029/98jd02651, 1998.

Piketh, S. J. and Walton, N. W.: Characteristics of Atmospheric Transport of Air Pollution for Africa, In: Stohl, A., ed., Intercontinental Transport of Air Pollution, Springer Berlin Heidelberg, 173-197, 2004.

Pochanart, P., Akimoto, H., Kajii, Y., and Sukasem, P.: Carbon monoxide, regional‐scale transport, and biomass burning in tropical continental Southeast Asia: Observations in rural Thailand, J. Geophys. Res., 108, 1337-1352, doi:doi:10.1029/2002JD003360, 2003.

Pochanart, P., Wild, O., and Akimoto, H.: Air pollution import to and export from East Asia, Air Pollution, 99-130, 2004.

Pulles, T., Bolscher, M. V. H., Brand, R., and Visschedijk, A.: Assessment of Global Emissions from Fuel Combustion in the Final Decades of the 20th Century, TNO report A-R0132/B, 2007.

Raper, J. L., Kleb, M. M., Jacob, D. J., Davis, D. D., Newell, R. E., Fuelberg, H. E., Bendura, R. J.,

Hoell, J. M., and McNeal, R. J.: Pacific Exploratory Mission in the Tropical Pacific- PEM-Tropics B, March-April 1999, J. Geophys. Res., 106, 32401-32425, doi:10.1029/2000JD900833, 2001.

980 Ridder, T., Gerbig, C., Notholt, J., Rex, M., Schrems, O., Warneke, T., and Zhang, L.: Ship-borne FTIR measurements of CO and O_3 in the Western Pacific from 43° N to 35° S: an evaluation of the sources, Atmos. Chem. Phys., 12, 815-828, doi:10.5194/acp-12-815-2012, 2012.

Rodríguez, S., Cuevas, E., Prospero, J., Alastuey, A., Querol, X., López-Solano, J., García, M., and Alonso-Pérez, S.: Modulation of Saharan dust export by the North African dipole, Atmos. Chem. Phys., 15, 7471-7486, doi:10.5194/acp-15-7471-2015, 2015.

985 Sauvage, B., Thouret, V., Cammas, J.-P., Gheusi, F., Athier, G., and Nédélec, P.: Tropospheric ozone over Equatorial Africa: regional aspects from the MOZAIC data, Atmos. Chem. Phys., 5, 311-335, doi:10.5194/acp-5-311-2005, 2005.

Sekiya, T., and Sudo, K.: Role of meteorological variability in global tropospheric ozone during 1970-2008, J. Geophys. Res., 117, D18303, doi:10.1029/2012JD018054, 2012.

990 Sekiya, T., and Sudo, K.: Roles of transport and chemistry processes in global ozone change on interannual and multidecadal time scales, J. Geophys. Res., 119, 4903-4921, doi:10.1002/2013JD020838, 2014.

Stein, A. F., Draxler, R. R., Rolph, G. D., Stunder, B. J. B., Cohen, M. D., and Ngan, F.: NOAA's HYSPLIT Atmospheric Transport and Dispersion Modeling System, Bull. Amer. Meteor. Soc., 96, 2059-2077, doi:10.1175/bams-d-14-00110.1, 2015.

Sudo, K., and Akimoto, H.: Global source attribution of tropospheric ozone: Long-range transport from various source regions, J. Geophys. Res., 112, D12302, doi:10.1029/2006JD007992, 2007.

Sultan, B., and Janicot, S.: Abrupt shift of the ITCZ over West Africa and intra-seasonal variability, Geophys. Res. Lett., 27, 3353-3356, doi:10.1029/1999gl011285, 2000.

1000 Suzuki, T.: Seasonal variation of the ITCZ and its characteristics over central Africa, Theor. Appl.

Climatol., 103, 39-60, doi:10.1007/s00704-010-0276-9, 2011.

Thompson, A. M.: Intercontinental Transport of Ozone from Tropical Biomass Burning, In: Stohl, A., ed., Intercontinental Transport of Air Pollution, Springer Berlin Heidelberg, 225-254, 2004.

Thompson, A. M., Miller, S. K., Tilmes, S., Kollonige, D. W., Witte, J. C., Oltmans, S. J., Johnson, B. J., Fujiwara, M., Schmidlin, F., and Coetzee, G.: Southern Hemisphere Additional Ozonesondes (SHADOZ) ozone climatology (2005-2009): Tropospheric and tropical tropopause layer (TTL) profiles with comparisons to OMI-based ozone products, J. Geophys. Res., 117, D23301, doi:10.1029/2011JD016911, 2012.

Thompson, A. M., Balashov, N. V., Witte, J., Coetzee, J., Thouret, V., and Posny, F.: Tropospheric ozone increases over the southern Africa region: bellwether for rapid growth in Southern Hemisphere pollution? Atmos. Chem. Phys., 14, 9855-9869, doi:10.5194/acp-14-9855-2014, 2014.

Van der Werf, G. R., Randerson, J. T., Giglio, L., Collatz, G. J., Mu, M., Kasibhatla, P. S., Morton, D. C., Defries, R. S., Jin, Y., and Leeuwen, T. T. V.: Global fire emissions and the contribution of deforestation, savanna, forest, agricultural, and peat fires (1997–2009), Atmos. Chem. Phys., 10, 16153-16230, doi:10.5194/acp-10-11707-2010, 2010.

Verstraeten, W. W., Neu, J. L., Williams, J. E., Bowman, K. W., Worden, J. R., and Boersma, K. F.: Rapid increases in tropospheric ozone production and export from China, Nat. Geosci., 8, 690-695, doi:10.1038/NGEO2493, 2015.

Vestreng, V., and Klein, H.: Emission data reported to UNECE/EMEP: Quality assurance and trend analysis & Presentation of WebDab, MSC-W Status Report 2002, Norwegian Meteorological Institute, Oslo Norway, July 2002.

Vogel, B., Günther, G., Müller, R., Grooß, J.-U., Hoor, P., Krämer, M., Müller, S., Zahn, A., and Riese, M.: Fast transport from Southeast Asia boundary layer sources to northern Europe: rapid uplift in typhoons and eastward eddy shedding of the Asian monsoon anticyclone, Atmos. Chem. Phys., 14,

1025   12745-12762, doi:10.5194/acp-14-12745-2014, 2014.

Waliser, D. E., and Gautier, C.: A satellite-derived climatology of the ITCZ, J. Climate, 6, 2162-2174, doi:10.1175/1520-0442(1993)006<2162:asdcot>2.0.co;2, 1993.

Waliser, D. E., Graham, N. E., and Gautier, C.: Comparison of the highly reflective cloud and outgoing longwave radiation datasets for use in estimating tropical deep convection, J. Climate, 6, 331-353,

1030   doi:10.1175/1520-0442(1993)006<0331:cothrc>2.0.co;2, 1993.

Wang, Y., Zhang, Y., Hao, J., and Luo, M.: Seasonal and spatial variability of surface ozone over China: contributions from background and domestic pollution, Atmos. Chem. Phys., 11, 3511-3525, doi:10.5194/acp-11-3511-2011, 2011.

Wild, O., Law, K. S., McKenna, D. S., Bandy, B. J., Penkett, S. A., and Pyle, J. A.: Photochemical

1035   trajectory modeling studies of the North Atlantic region during August 1993, J. Geophys. Res., 101, 29269-29288, doi:10.1029/96jd00837, 1996.

Wild, O., Pochanart, P., and Akimoto, H.: Trans-Eurasian transport of ozone and its precursors, J. Geophys. Res., 109, D11302, doi:10.1029/2003JD004501, 2004.

Williams, J., Scheele, M., Van Velthoven, P., Cammas, J.-P., Thouret, V., Galy-Lacaux, C., and Volz-

1040   Thomas, A.: The influence of biogenic emissions from Africa on tropical tropospheric ozone during 2006: a global modeling study, Atmos. Chem. Phys., 9, 5729-5749, doi:10.5194/acp-9-5729-2009, 2009.

Xie, S.-P.: The shape of continents, air-sea interaction, and the rising branch of the Hadley circulation, in: The Hadley Circulation: Present, Past and Future, Springer, 121-152, 2004.

1045   Yevich, R., and Logan, J. A.: An assessment of biofuel use and burning of agricultural waste in the developing world, Global Biogeochem. Cy., 17, 1095, doi:10.1029/2002GB001952, 2003.

Žagar, N., Skok, G., and Tribbia, J.: Climatology of the ITCZ derived from ERA Interim reanalyses, J. Geophys. Res., 116, D15103, doi:10.1029/2011JD015695, 2011.

Zare, A., Christensen, J. H., Gross, A., Irannejad, P., Glasius, M., and Brandt, J.: Quantifying the

1050   contributions of natural emissions to ozone and total fine PM concentrations in the Northern

Hemisphere, Atmos. Chem. Phys., 14, 2735-2756, doi:10.5194/acp-14-2735-2014, 2014.

Zhang, G. J., and McFarlane, N. A.: Sensitivity of climate simulations to the parameterization of

cumulus convection in the Canadian climate centre general circulation model, Atmos. Ocean., 33,

407-446, doi:10.1080/07055900.1995.9649539, 1995.

1055 Zhang, L., Li, Q. B., Jin, J., Liu, H., Livesey, N., Jiang, J. H., Mao, Y., Chen, D., Luo, M., and Chen, Y.:

Impacts of 2006 Indonesian fires and dynamics on tropical upper tropospheric carbon monoxide and

ozone, Atmos. Chem. Phys., 11, 10929-10946, doi:10.5194/acp-11-10929-2011, 2011.

Zhang, L., Jacob, D. J., Boersma, K. F., Jaffe, D. A., Olson, J. R., Bowman, K. W., Worden, J. R.,

Thompson, A. M., Avery, M. A., Cohen, R. C., Dibb, J. E., Flock, F. M., Fuelberg, H. E., Huey, L. G.,

1060 McMillan, W. W., Singh, H. B., and Weinheimer, A. J.: Transpacific transport of ozone pollution and

the effect of recent Asian emission increases on air quality in North America: an integrated analysis

using satellite, aircraft, ozonesonde, and surface observations, Atmos. Chem. Phys., 8, 6117-6136,

doi:10.5194/acp-8-6117-2008, 2008.

Zhang, Q., Streets, D. G., Carmichael, G. R., He, K. B., Huo, H., Kannari, A., Klimont, Z., Park, I. S.,

1065 Reddy, S., Fu, J. S., Chen, D., Duan, L., Lei, Y., Wang, L. T., and Yao, Z. L.: Asian emissions in 2006

for the NASA INTEX-B mission, Atmos. Chem. Phys., 9, 5131-5153, doi:10.5194/acp-9-5131-2009,

2009.

Zhao, T., Gong, S., Zhang, X., and McKendry, I.: Modeled size-segregated wet and dry deposition

budgets of soil dust aerosol during ACE-Asia 2001: Implications for trans-Pacific transport, J.

1070 Geophys. Res., 108, 420-424, doi:10.1029/2002JD003363, 2003.

Zhu, Y.: Variations of the summer Somali and Australia cross-equatorial flows and the implications for

the Asian summer monsoon, Adv. Atmos. Sci., 29(3), 509-518, doi:10.1007/s00376-011-1120-6,

2012.

Zhu, B., Hou, X., and Kang, H.: Analysis of the seasonal ozone budget and the impact of the summer
monsoon on the northeastern Qinghai-Tibetan Plateau, J. Geophys. Res., 121, 2029-2042,
doi:10.1002/2015JD023857, 2016.

Zhu, J., Liao, H., Mao, Y., Yang, Y., and Jiang, H.: Interannual variation, decadal trend, and future
change in ozone outflow from East Asia, Atmos. Chem. Phys., 17, 3729-3747, doi:10.5194/acp-17-
3729-2017, 2017a.

Zhu, Y., Liu, J., Wang, T., Zhuang, B., Han, H., Wang, H., Chang, Y., and Ding, K.: The impacts of
meteorology on the seasonal and interannual variabilities of ozone transport from North America to
East Asia, J. Geophys. Res., 122, doi:10.1002/2017JD026761, 2017b.
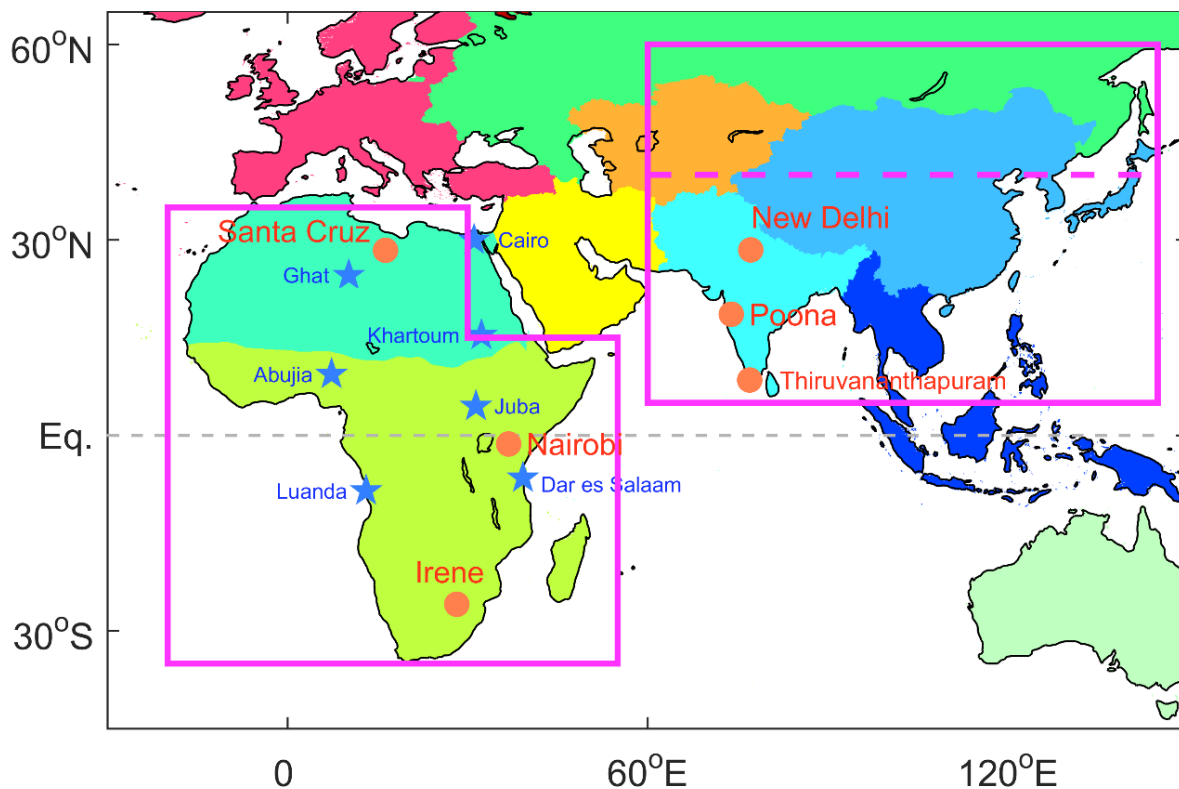
Figure 1. Domains of the source region, Africa, and the receptor region, Asia (areas within the solid purple lines). The area at the latitudes south to the pink dashed line at 40°N in Asia is used for the regional mean of Asia for Figs. 6, 7, 14 and 15. The brown dots indicate the locations of the ozonesonde sites where the ozone measurements are compared with the GEOS-Chem simulations. The seven blue stars indicate the sites where forward trajectory simulations are originated. The color-filled continents stand for the source regions defined in the HTAP Phase 2 (HTAP2).
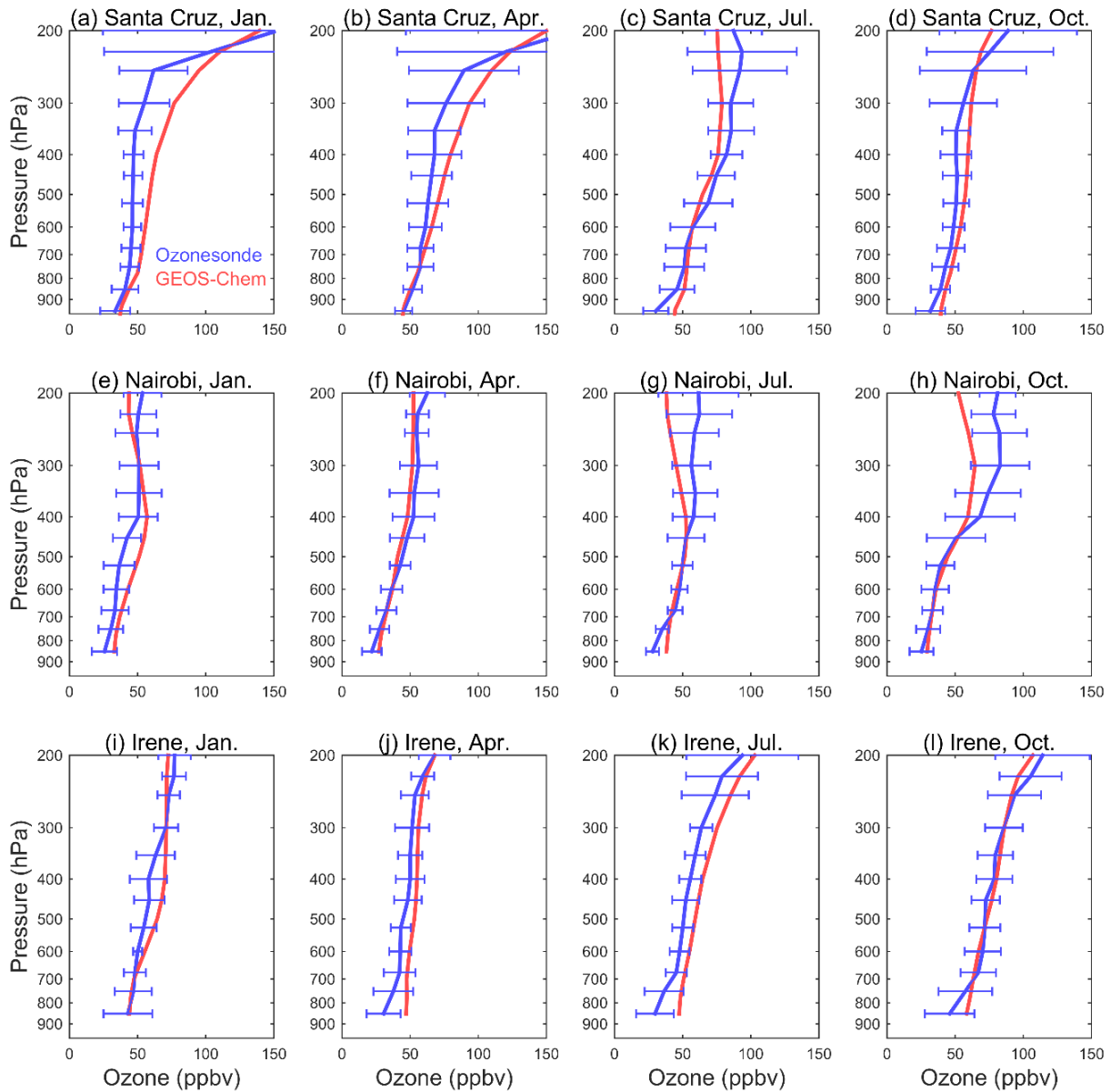
Figure 2. Comparison of the monthly mean ozone vertical profiles between the GEOS-Chem simulations (red line) and the ozonesonde measurements (blue line) averaged over 1999-2003 at Santa Cruz (1st row), 2003-2006 for Nairobi (2nd row), 1999-2005 for Irene (3rd row), in January (1st col.), April (2nd col.), July (3rd col.), and October (4th col.), respectively. The horizontal bar indicates the standard deviation.
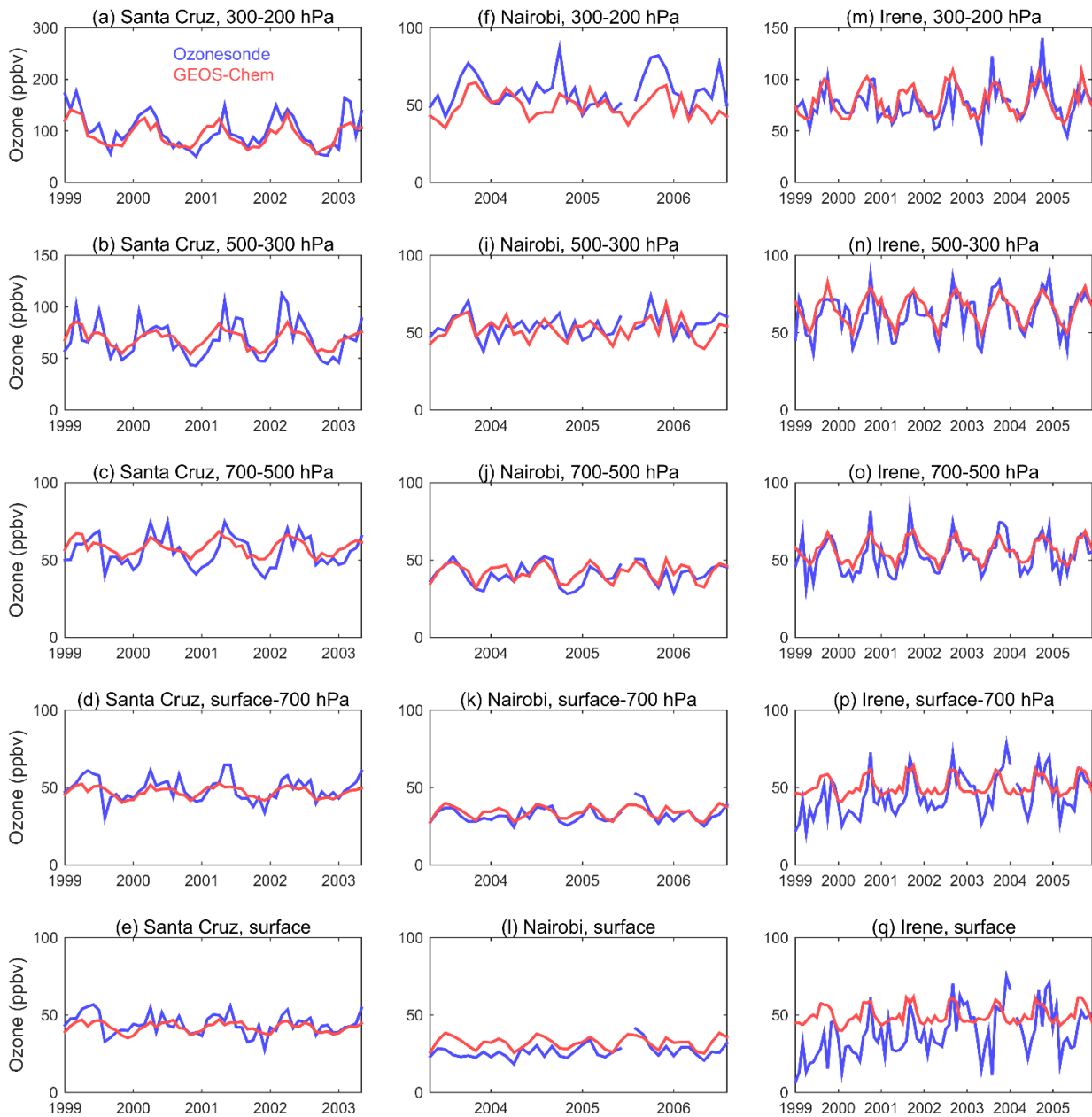
Figure 3. Comparison of the time series of monthly ozone between GEOS-Chem simulations (red line) and ozonesonde measurements (blue line) for layers averaged over 300-200 hPa (1st row), 500-300 hPa (2nd row), 700-500 hPa (3rd row), surface-700 hPa (4th row), and at the surface layer (5th row) at Santa Cruz (1st col.), Nairobi (2nd col.), and Irene (3rd col.) in Africa, respectively.
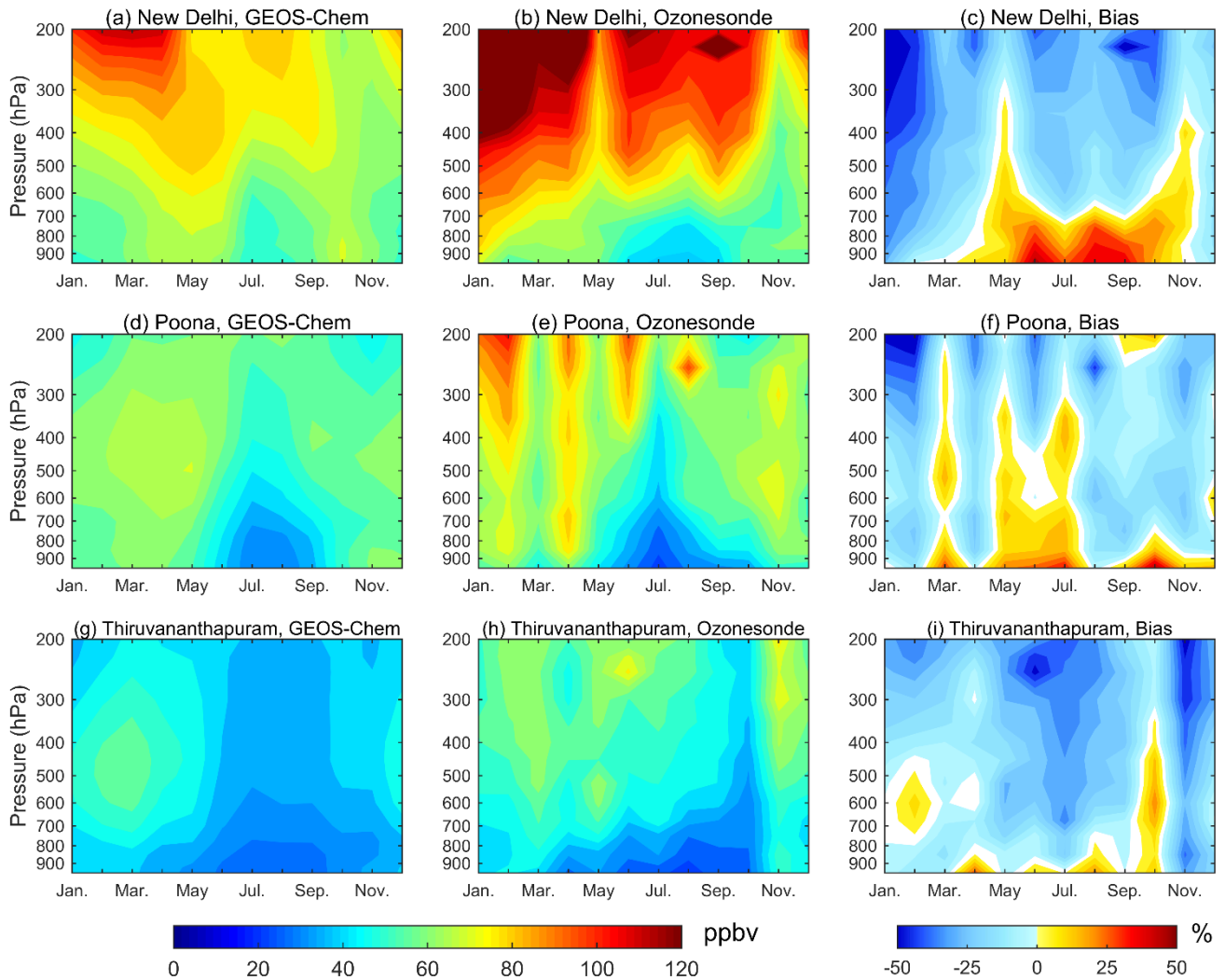
Figure 4. Seasonal variation of vertical profiles of ozone (in ppbv) from the GEOS-Chem simulations (1st col), ozonesonde measurements (2nd col.), and the corresponding bias (in %, 3rd col.) averaged over 1994-2003 at the Indian three sites, New Delhi (1st row), Poona (2nd row), and Thiruvananthapuram (3rd row) in India.

1140
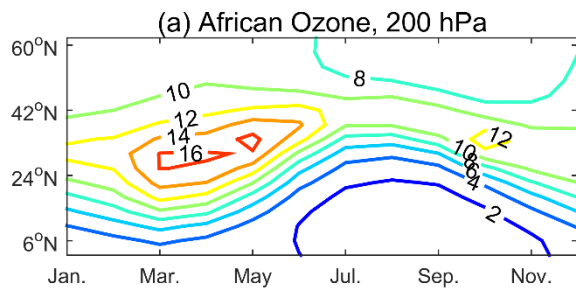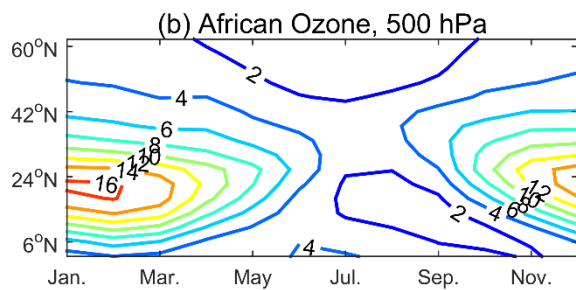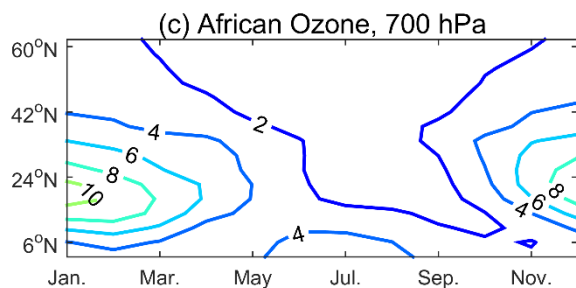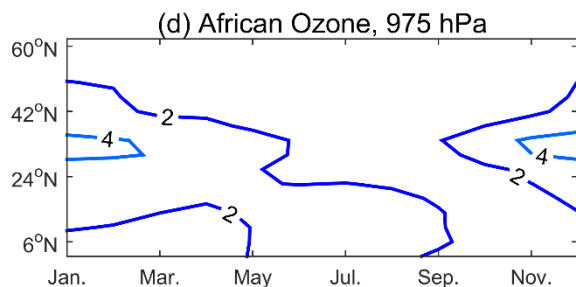
1145
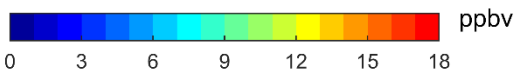
Figure 5. Seasonal variation of imported African ozone (in ppbv) over Asia varying with latitude at (a) 200 hPa, (b) 500 hPa, (c) 700 hPa, and (d) 975 hPa. The values are the 20-year means (1987-2006) from the GEOS-Chem simulation and averaged over 60-145°E.
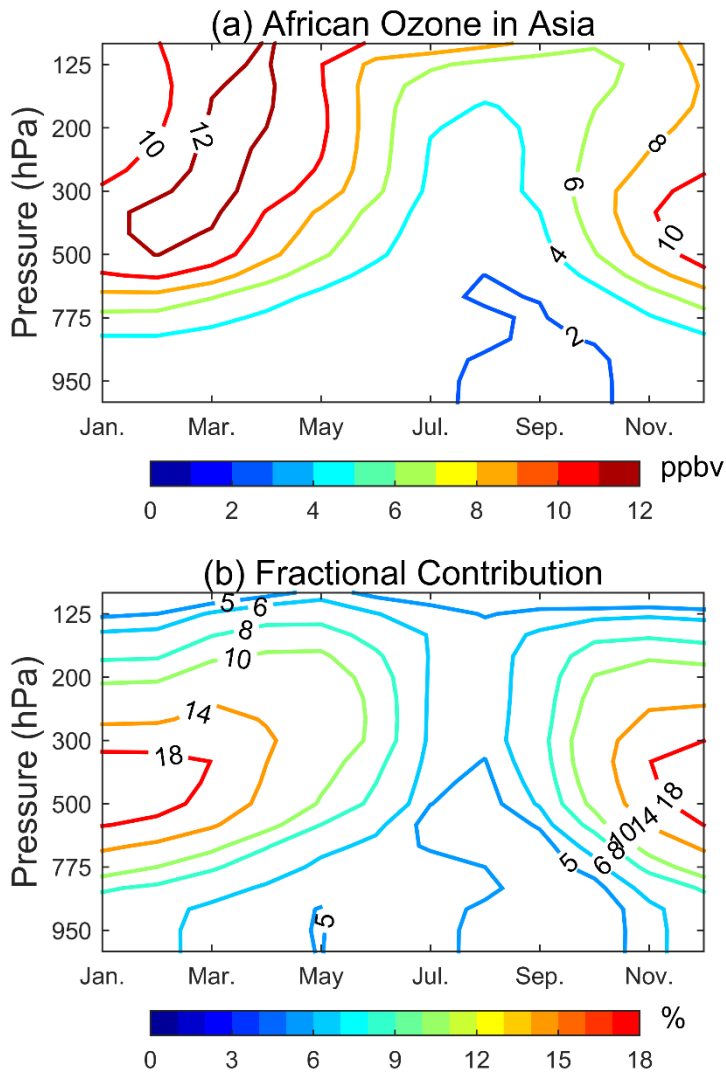
Figure 6. (a) Seasonal variation of imported African ozone (in ppbv) varying with altitude. (b) The same as (a) but for the corresponding fractional contribution (in %). The values are the 20-year means (1987-2006) from the GEOS-Chem simulation and averaged over Asia (60-145°E, 5-40°N, see Fig. 1).
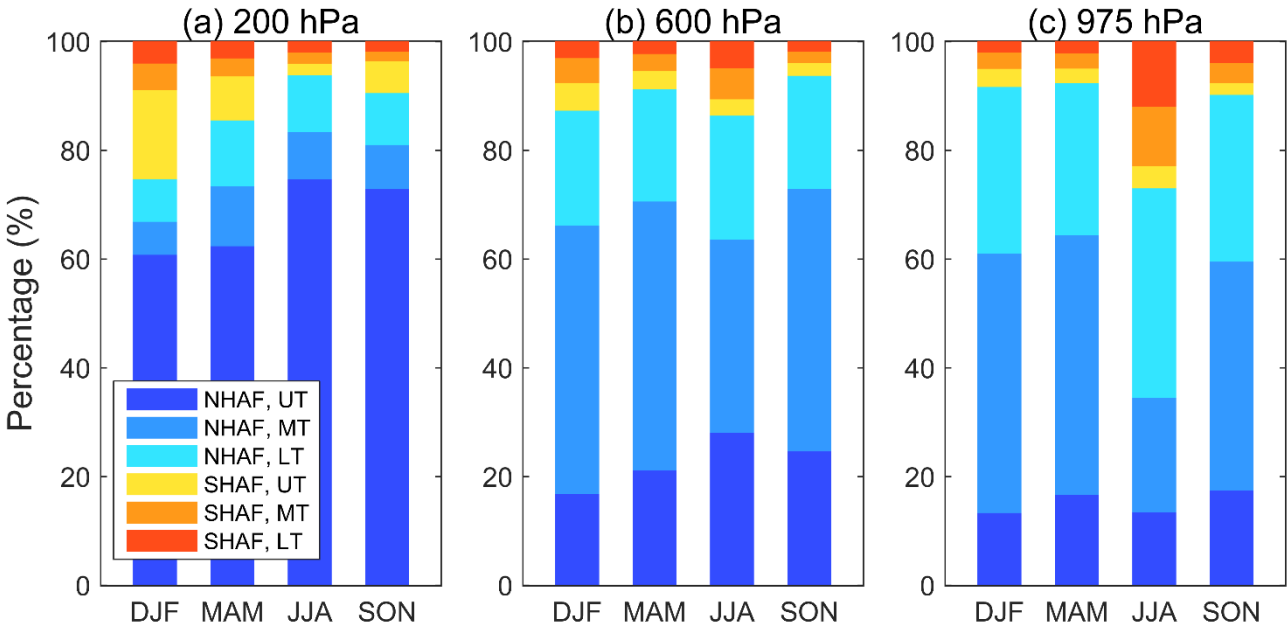
Figure 7. The fractional contribution of the imported African ozone over Asia from a layer in Africa to the total imported Africa ozone from all layers (in %). The layers include the lower troposphere (LT), middle troposphere (MT), and upper troposphere (UT). Each layer is further separated by hemisphere with blueish color for NHAF and reddish color for SNAF. The fractional contribution is shown in the bars by season at (a) 200 hPa, (b) 600 hPa, and (c) 975 hPa over Asia. The values are the 20-year means (1987-2006) from the GEOS-Chem simulation and averaged over Asia (60-145°E, 5-40°N, see Fig. 1).

(a) Biogenic Isoprene, Jan.　(b) Biogenic Isoprene, Apr.　(c) Biogenic Isoprene, Jul.　(d) Biogenic Isoprene, Oct.

10^{12} atoms C cm^{-2} s^{-1}
0　2.5　5

(e) CO from Biomass Burning, Jan.　(f) CO from Biomass Burning, Apr.　(g) CO from Biomass Burning, Jul.　(h) CO from Biomass Burning, Oct.

10^{12} molec cm^{-2} s^{-1}
0　4　8

(i) Lightning NOx, 300 hPa, Jan.　(j) Lightning NOx, 300 hPa, Apr.　(k) Lightning NOx, 300 hPa, Jul.　(l) Lightning NOx, 300 hPa, Oct.

10^{10} molec m^{-3} s^{-1}
0　2　4

(m) Lightning NOx, 700 hPa, Jan.　(n) Lightning NOx, 700 hPa, Apr.　(o) Lightning NOx, 700 hPa, Jul.　(p) Lightning NOx, 700 hPa, Oct.

10^{10} molec m^{-3} s^{-1}
0　2　4

1205   Figure 8. Distributions of isoprene emissions from biogenic sources (1st row), CO emissions from biomass burning (2nd row) and NO_x emissions from lightning at 300 hPa (3rd row) and 700 hPa (4th row) by season in 2005. The data are based on the emission inventories in GEOS-Chem (see section 2.1). The dash lines indicate the equator. The black solid lines indicate the seasonal variation in the locationof the ITCZ.

1210
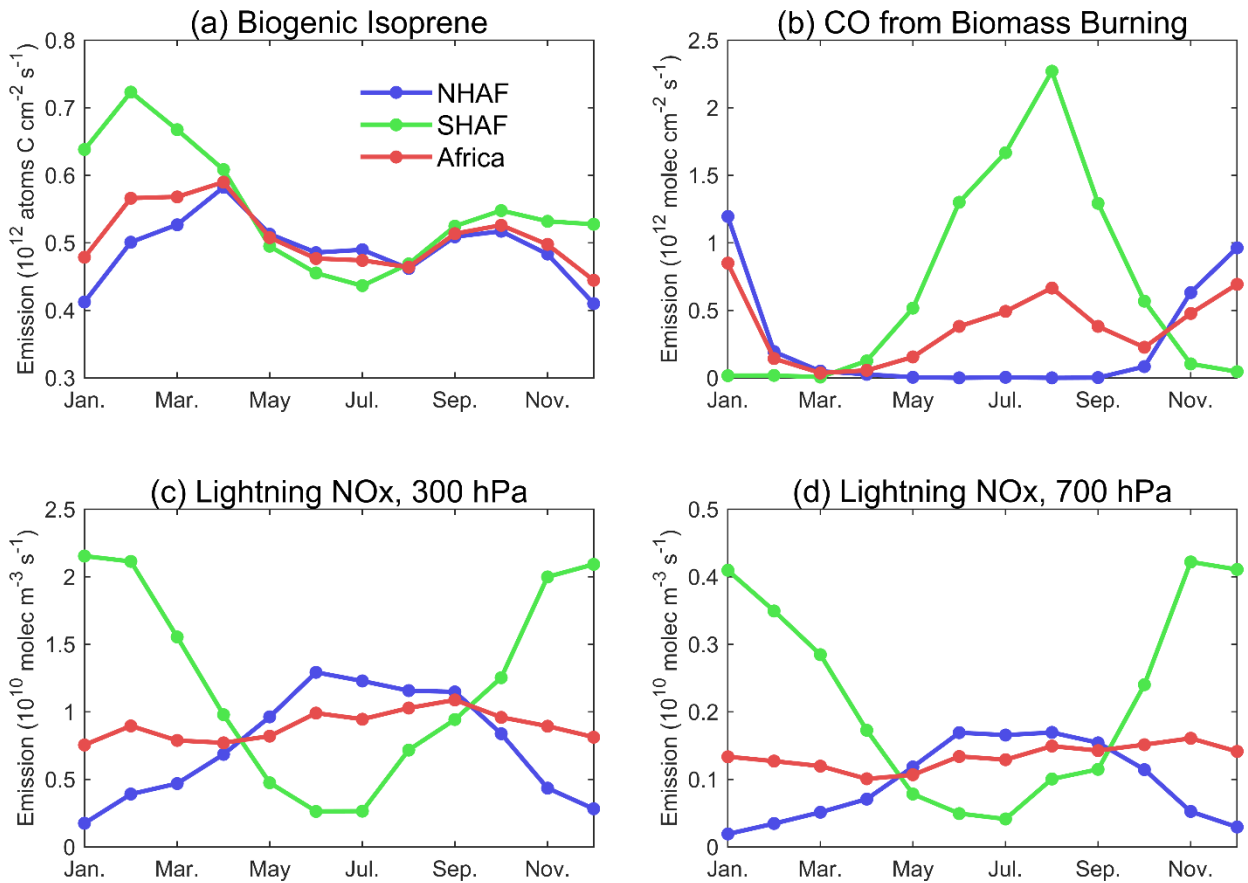
1215

Figure 9. Seasonal variations for (a) isoprene emissions from biogenic sources, (b) CO emissions from biomass burning, NO_x emissions from lightning at (c) 300 hPa, and (d) 700 hPa averaged over Africa, NHAF and SHAF in 2005.
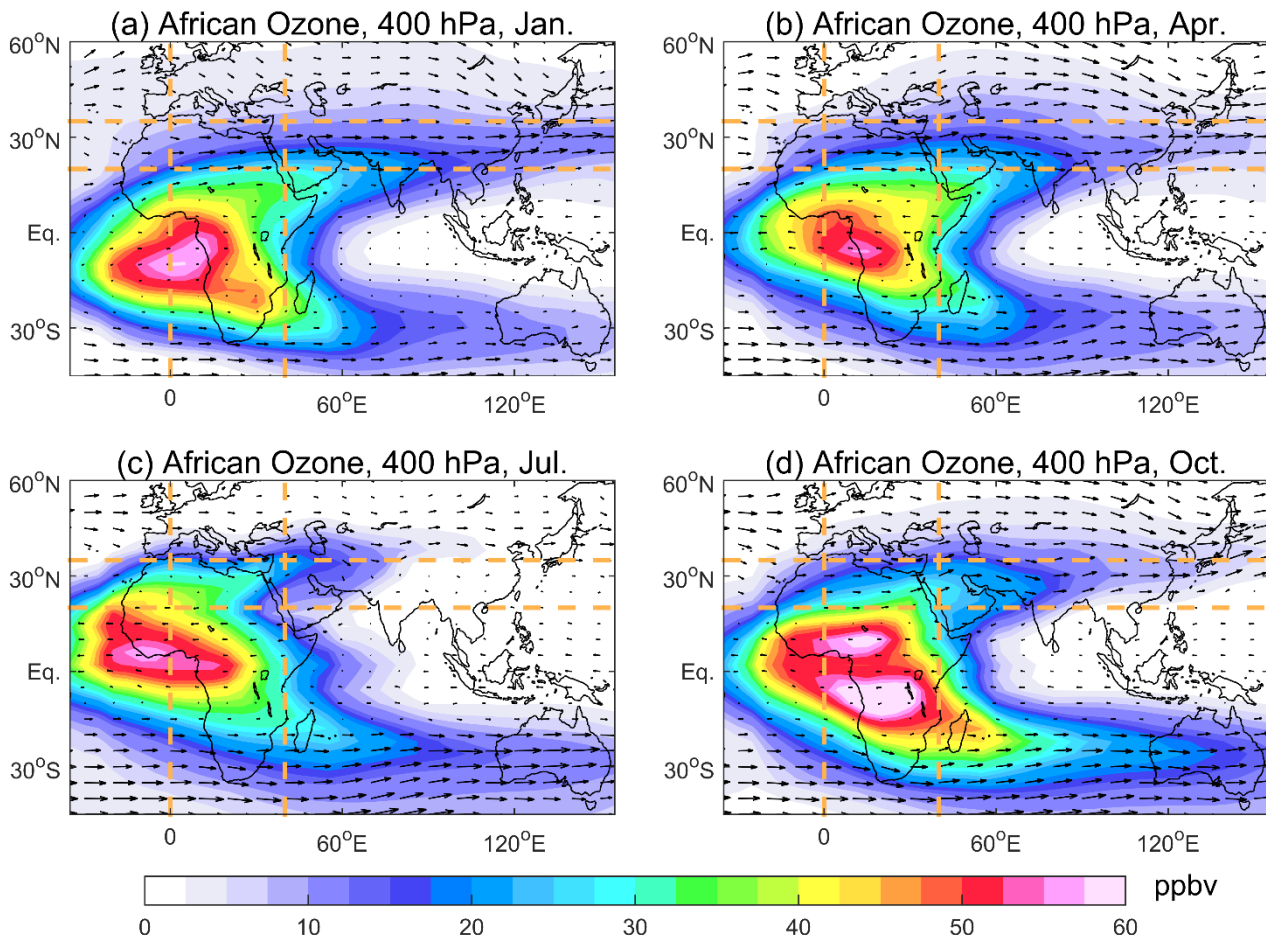
Figure 10. Horizontal distributions of African ozone (in ppbv, in color) overlaid with winds (in arrow) at 400 hPa in (a) January, (b) April, (c) July, and (d) October. The ozone values are the means from the 20-year GEOS-Chem simulation. The between the two pairs of parallel dished lines, latitudinal and longitudinal means are taken and shown in Fig. 11 and Fig. 12, respectively

1225

1230
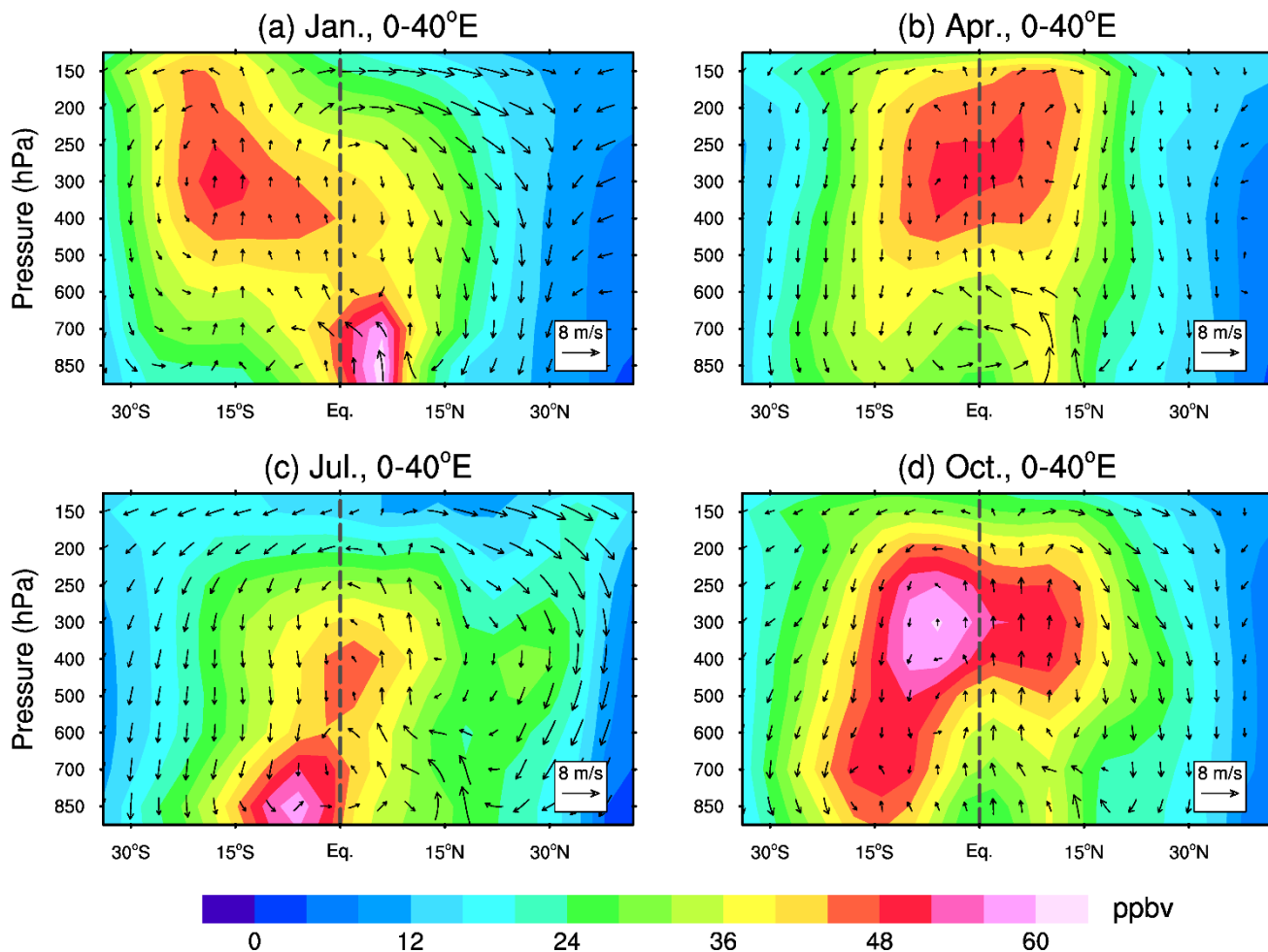
Figure 11. Latitude-altitude distribution of African ozone (in ppbv, in color), overlaid with winds (in arrow) in (a) January, (b) April, (c) July, and (d) October. The ozone values are the means over 0-40°E (see Figure 10) from the 20-year GEOS-Chem simulation. The vertical velocities in the p-coordinates are enlarged by 100 times for illustration purposes.
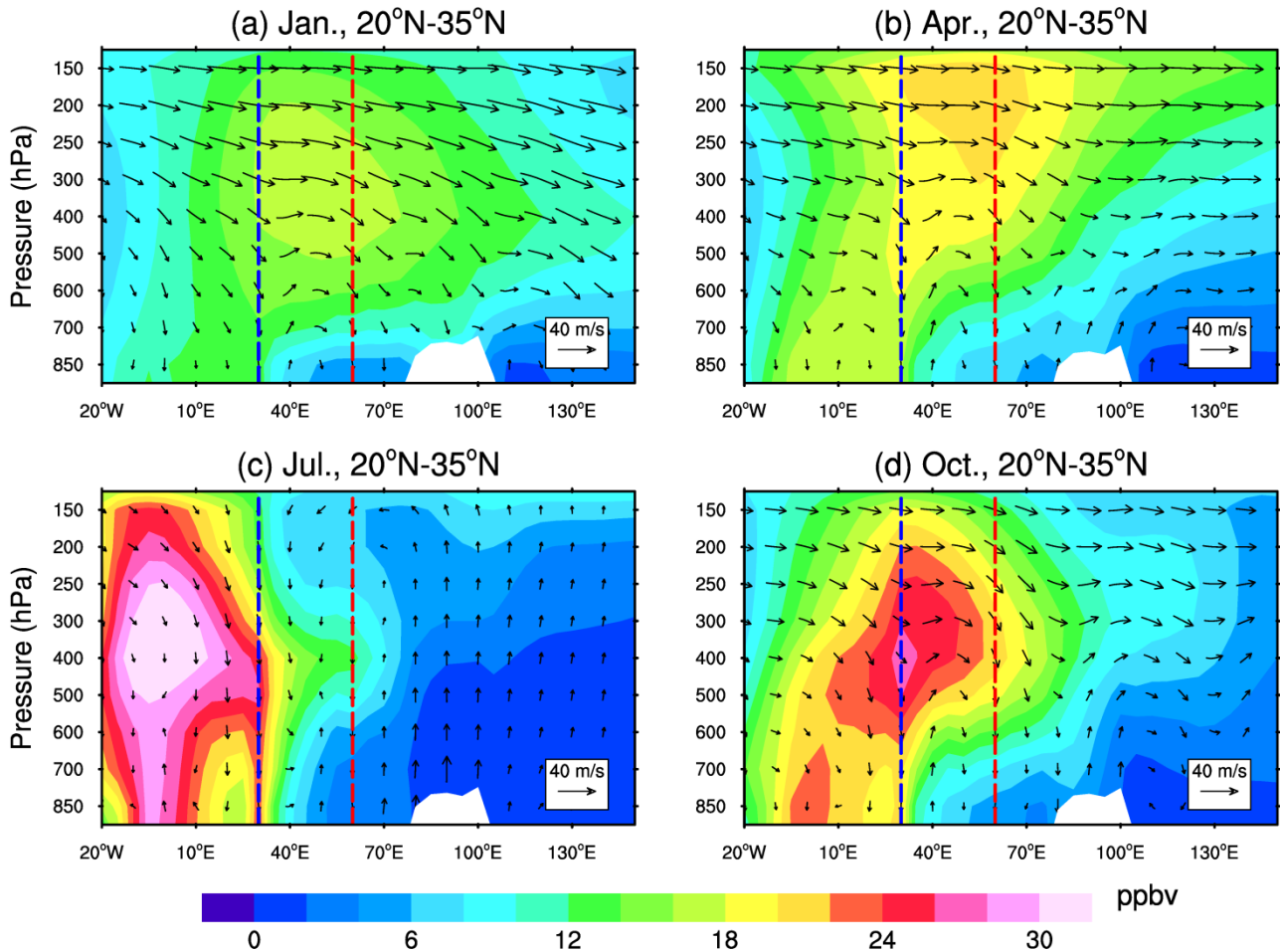
Figure 12. Longitude-altitude distribution of African ozone (in ppbv, in color), overlaid with winds (in arrow) in (a) January, (b) April, (c) July, and (d) October. The ozone values are the means over 25°N-30°N (see Figure 10) from the 20-year GEOS-Chem simulation. White areas indicate topography. The red and blue dash lines indicate the western border of Asia and eastern border of Africa, respectively. The vertical velocities in the p-coordinates are enlarged by 100 times for illustration purposes.
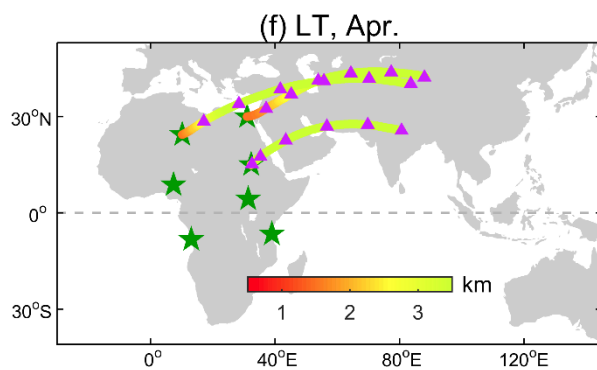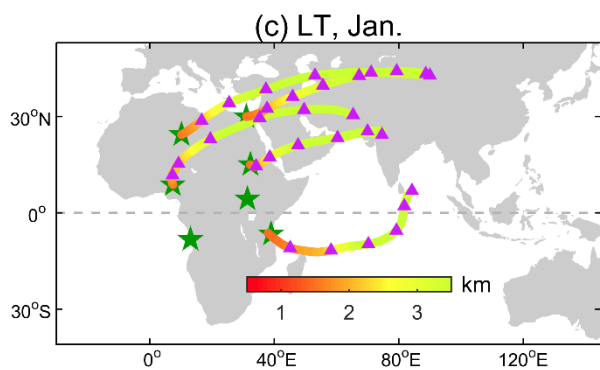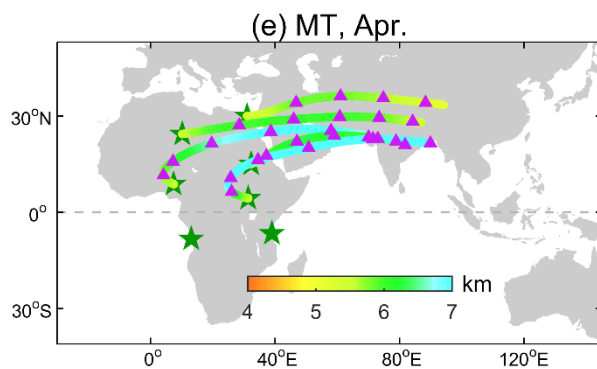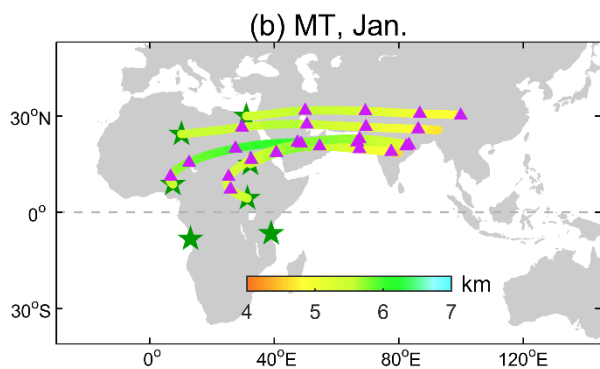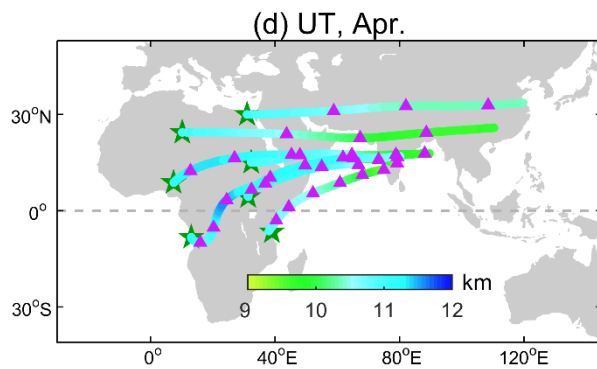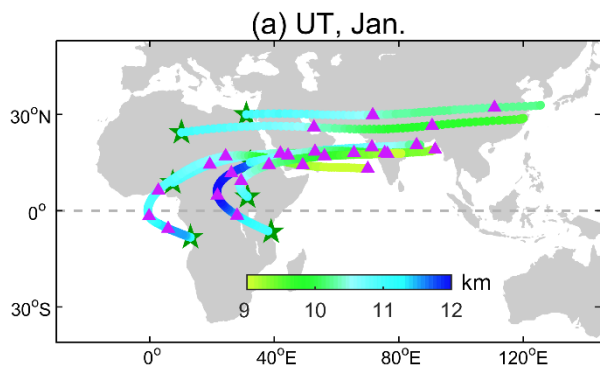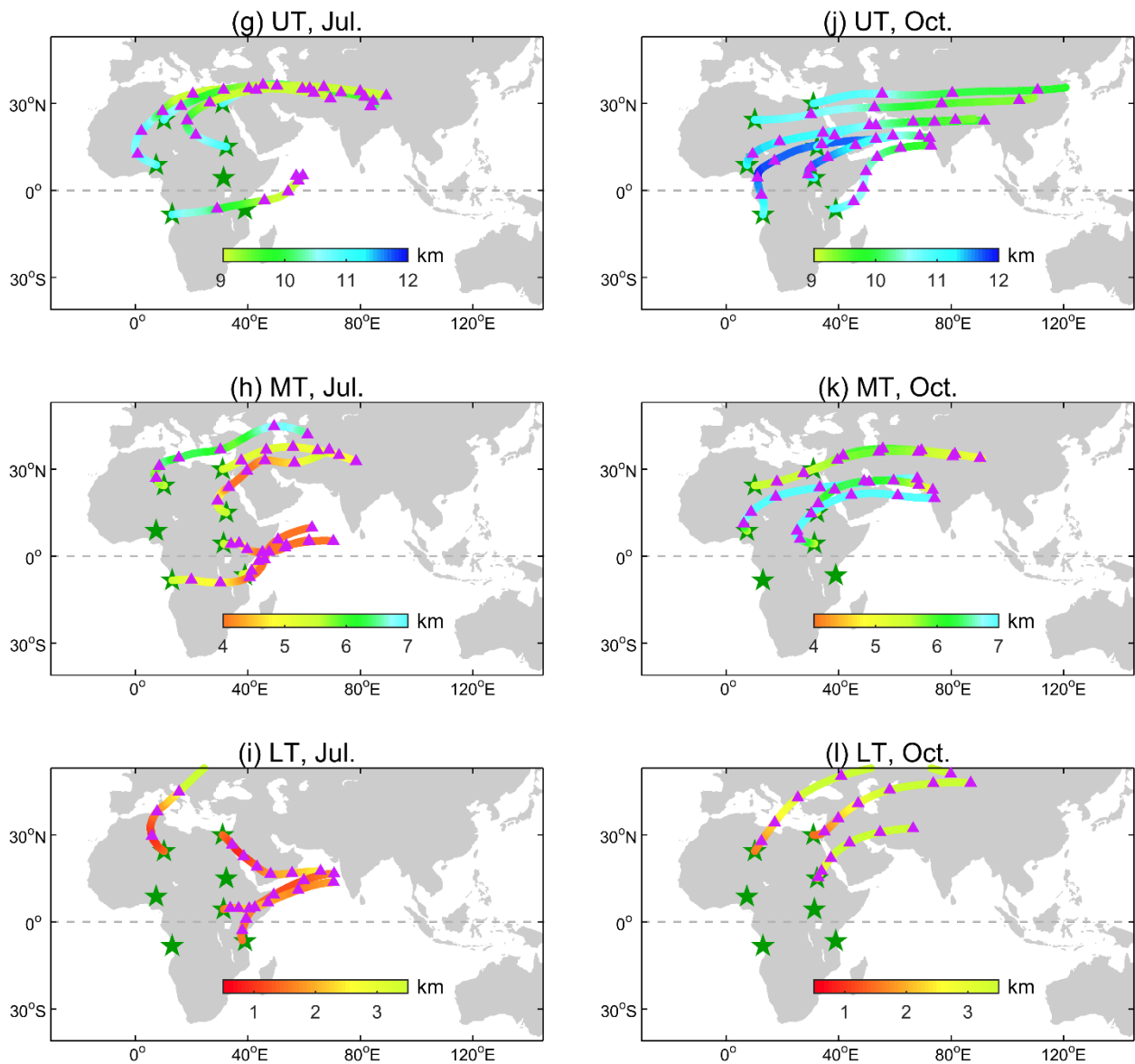
Figure 13. Mean seasonal paths for the trajectories that reach Asia and originated from the African sites at Cairo, Ghat, Abuja, Khartoum, Juba, Dar es Salaam, and Luanda in Africa (stars, also see Fig. 1) from 11 km (1st row), 5.5 km (2nd row), and 1.5 km (3rd row) in January (1st col.), April (2nd col.), July (3rd col.), and October (4th col.) between period 1987- 2006. The triangles along the trajectory paths indicate the lapse days from the beginning.
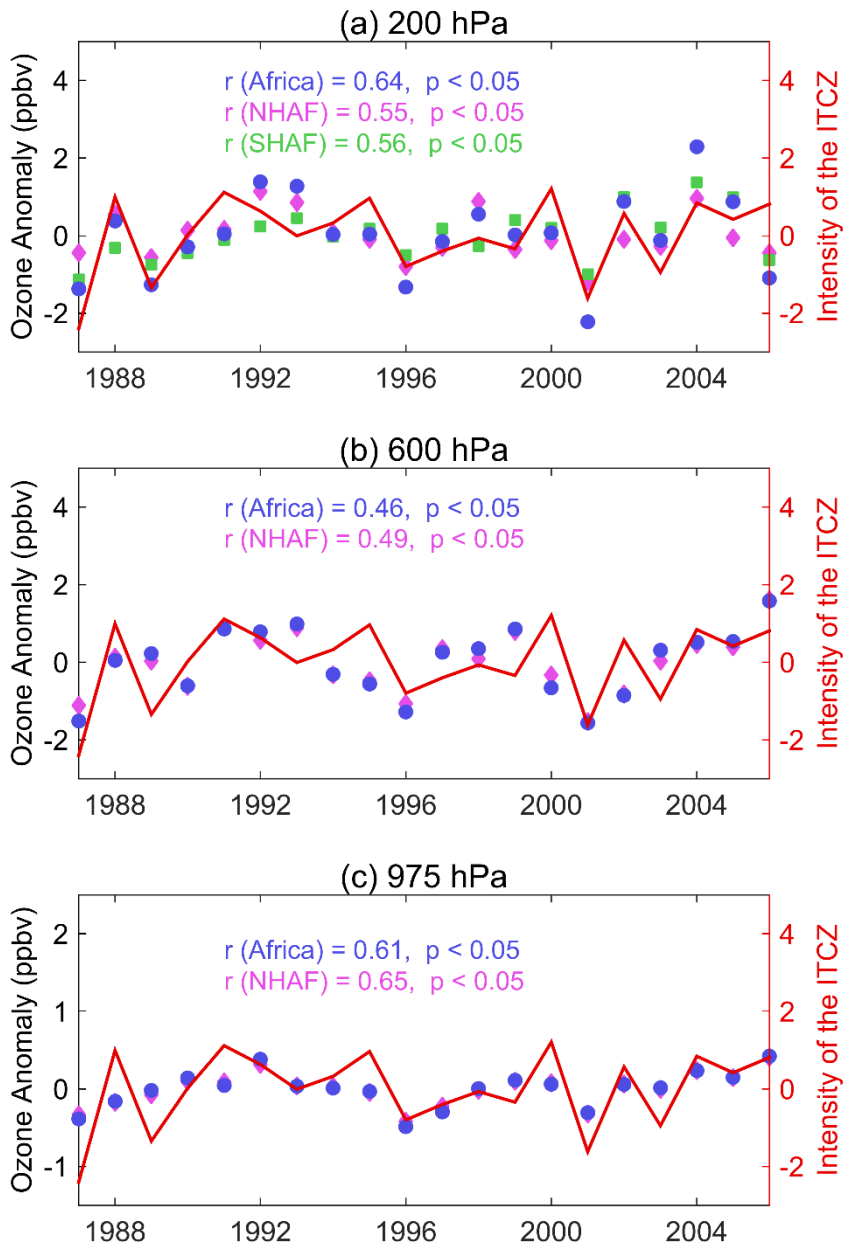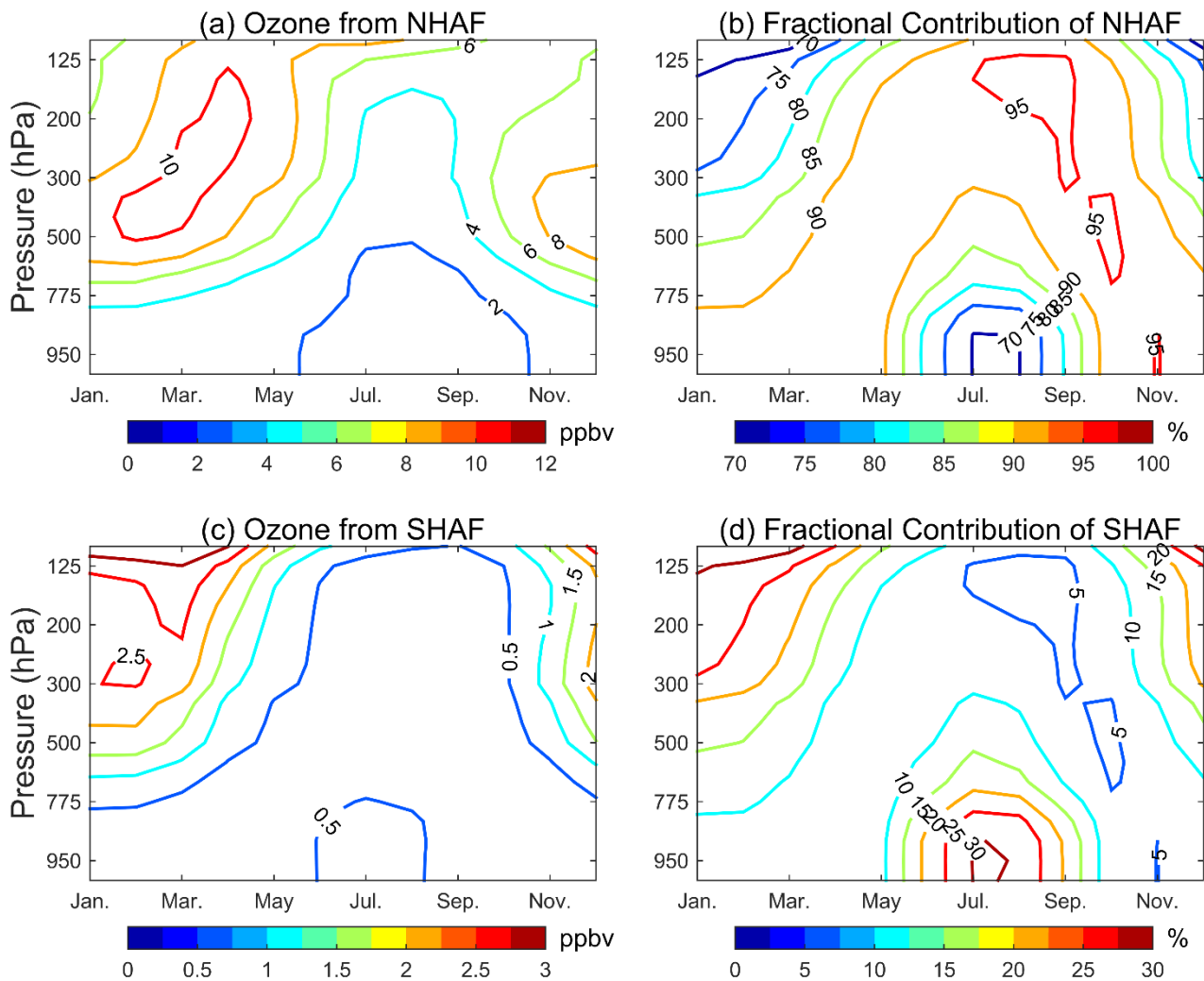
Figure 14. Interannual variation of the intensity of ITCZ (the values are normalized) over Africa and the anomaly of imported ozone from Africa, NHAF and SHAF over Asia from 1987 to 2006 at (a) 200 hPa, (b) 600 hPa, and (c) 975 hPa in January, respectively.

Figure 15. Seasonal-altitude variations of imported ozone (in ppbv) from (a) NHAF and (c) SHAF over Asia (60-145°E, 5-40°N, see Fig. 1) and the fractional contribution of ozone from (b) NHAF and (d) SHAF to the total African ozone over Asia (in %). The ozone values are the means from the 20-year GEOS-Chem simulation.
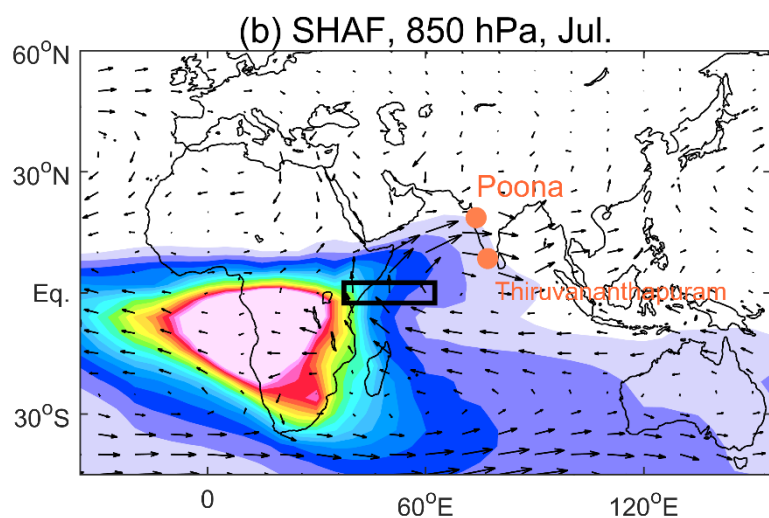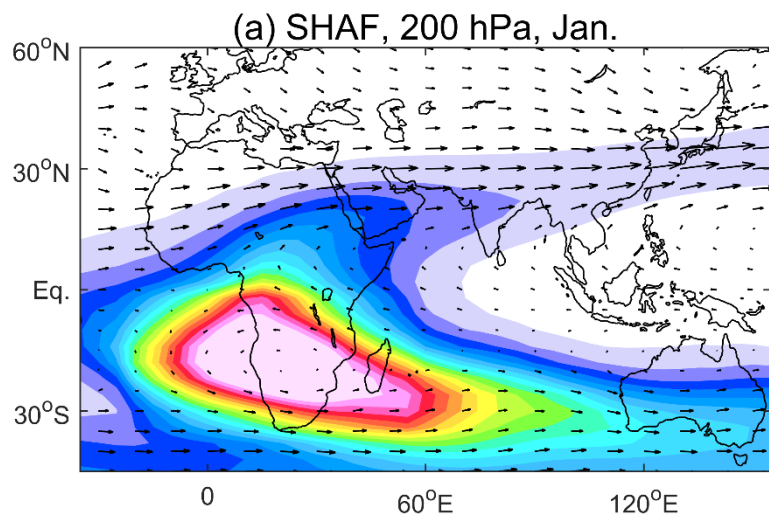
Figure 16. Distributions of ozone from SHAF (in ppbv, in color) overlaid with winds (in arrow) at (a) 200 hPa in January and (b) at 925 hPa in July. The ozone values are the means from the 20-year GEOS-Chem simulation. The black rectangle indicates the domain used in calculating the strength of the Somali cross-equatorial flow. The brown dots indicate the ozonesonde sites in western India.

1275

1280
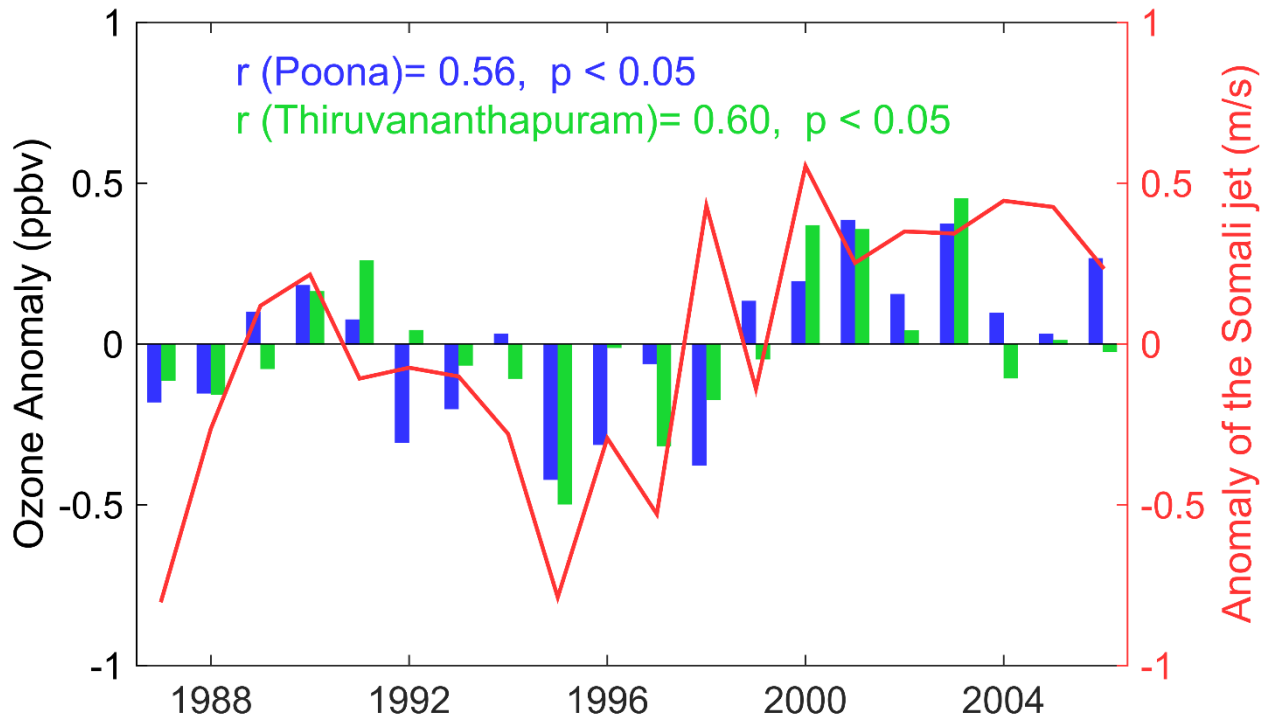
1285

Figure 17. Interannual variation of the anomaly of ozone from SHAF at two Indian sites, Poona and Thiruvananthapuram in the lower troposphere in NH summer and the strength of the Somali jet from 1987 to 2006.

1290

Table 1. The ozone profiles (see Fig. 2) simulated with GESOS-Chem in comparison with the ozonesonde measurements at Santa Cruz, Nairobi, and Irene in Africa in terms of bias (in %), root-mean-square error (RMSE, in ppbv), and correlation coefficient (r) in the four seasons.

	Month	Jan.	Apr.	Jul.	Oct.
Santa Cruz	r	0.94	0.95	0.98	0.95
	Bias (%)	23.2	8.8	-1.6	9.1
	RMSE (ppbv)	15.5	11.8	9.2	7.0
	Month	Jan.	Apr.	Jul.	Oct.
Nairobi	r	0.69	0.99	0.26	0.94
	Bias (%)	10.7	-2.3	-9.1	-9.3
	RMSE (ppbv)	7.6	4.3	12.3	14.2
	Month	Jan.	Apr.	Jul.	Oct.
Irene	r	0.89	0.97	0.99	0.97
	Bias (%)	5.0	15.6	20.9	1.8
	RMSE (ppbv)	5.9	7.5	10.9	5.5

Table 2. The time series of ozone concentrations at different tropospheric layers (see Fig. 3) from the GESOS-Chem simulations and ozonesonde measurements at Santa Cruz, Nairobi, and Irene in Africa. The two datasets are compared in terms of bias (in %), root-mean-square error (RMSE, in ppbv), and correlation coefficient (r).

	Layer	300-200 hPa	500-300 hPa	700-500 hPa	Surface-700 hPa	Surface Layer
Santa Cruz	r	0.79	0.75	0.57	0.62	0.60
	Bias (%)	-4.2	7.1	7.3	-2.3	-2.7
	RMSE (ppbv)	22.9	12.7	8.4	6.3	5.6
	Layer	300-200 hPa	500-300 hPa	700-500 hPa	Surface-700 hPa	Surface Layer
Nairobi	r	0.76	0.79	0.85	0.90	0.82
	Bias (%)	-14.2	-3.3	4.9	6.5	22.8
	RMSE (ppbv)	13.0	7.4	5.1	3.5	6.6
	Layer	300-200 hPa	500-300 hPa	700-500 hPa	Surface-700 hPa	Surface Layer
Irene	r	0.70	0.82	0.82	0.61	0.39
	Bias (%)	5.7	7.3	8.6	20.7	60.3
	RMSE (ppbv)	13.6	8.6	7.8	12.3	18.7

1305